Low-Frequency Weather and the Emergence of the Climate

S. Lovejoy

Department of Physics, McGill University, Montreal, Quebec, Canada

D. Schertzer

LEESU, Ecole des Ponts ParisTech, Université Paris Est, Paris, France
Météo France, Paris, France

We survey atmospheric variability from weather scales up to several hundred kiloyears. We focus on scales longer than the critical $\tau_w \approx 5$–20 day scale corresponding to a drastic transition from spectra with high to low spectral exponents. Using anisotropic, intermittent extensions of classical turbulence theory, we argue that τ_w is the lifetime of planetary-sized structures. At τ_w, there is a dimensional transition; at longer times the spatial degrees of freedom are rapidly quenched, leading to a scaling "low-frequency weather" regime extending out to $\tau_c \approx 10$–100 years. The statistical behavior of both the weather and low-frequency weather regime is well reproduced by turbulence-based stochastic models and by control runs of traditional global climate models, i.e., without the introduction of new internal mechanisms or new external forcings; hence, it is still fundamentally "weather." Whereas the usual (high frequency) weather has a fluctuation exponent $H > 0$, implying that fluctuations *increase* with scale, in contrast, a key characteristic of low-frequency weather is that $H < 0$ so that fluctuations *decrease* instead. Therefore, it appears "stable," and averages over this regime (i.e., up to τ_c) define climate *states*. However, at scales beyond τ_c, whatever the exact causes, we find a new scaling regime with $H > 0$; that is, where fluctuations again *increase* with scale, climate states thus appear unstable; this regime is thus associated with our notion of *climate change*. We use spectral and difference and Haar structure function analyses of reanalyses, multiproxies, and paleotemperatures.

1. INTRODUCTION

1.1. What Is the Climate?

Notwithstanding the explosive growth of climate science over the last 20 years, there is still no clear universally accepted definition of what the climate *is* or what is almost the same thing, what distinguishes the weather from the climate. The core idea shared by most climate definitions is famously encapsulated in the dictum: "The climate is what you expect, the weather is what you get" (see *Lorenz* [1995] for a discussion). In more scientific language, "Climate in a narrow sense is usually defined as the average weather, or more rigorously, as the statistical description in terms of the mean and variability of relevant quantities over a period of time ranging from months to thousands or millions of years" [*Intergovernmental Panel on Climate Change*, 2007, p. 942].

An immediate problem with these definitions is that they fundamentally depend on subjectively defined averaging scales. While the World Meteorological Organization defines climate as 30 years or longer variability, a period of 2 weeks to a month is commonly used to distinguish weather from climate so that even with these essentially arbitrary periods, there is still a range of about a factor 1000 in scale (2 weeks to 30 years) that is up in the air. This fuzzy distinction is also reflected in numerical climate modeling since global climate models are fundamentally the same as weather models but at lower resolutions, with a different assortment of subgrid parametrizations, and they are coupled to ocean models and, increasingly, to cryosphere, carbon cycle, and land use models. Consequently, whether we define the climate as the long-term weather statistics, or in terms of the long-term interactions of components of the "climate system," we still need an objective way to distinguish it from the weather. These problems are compounded when we attempt to objectively define climate *change*.

However, there is yet another problem with this and allied climate definitions: they imply that climate dynamics are nothing new, that they are simply weather dynamics at long time scales. This seems naïve since we know from physics that when processes repeat over wide-enough ranges of space or time scales, qualitatively new low-frequency laws should emerge. These "emergent" laws could simply be the consequences of long-range statistical correlations in the weather physics in conjunction with qualitatively new climate processes, due to either internal dynamics or to external forcings, their nonlinear synergy giving rise to emergent laws of climate dynamics.

1.2. Using the Type of Scaling Variability to Determine the Dynamical Regime

The atmosphere is a nonlinear dynamical system with interactions and variability occurring over huge ranges of space and time scales (millimeters to planet scales, milliseconds to billions of years, ratios $\approx 10^{10}$ and $\approx 10^{20}$, respectively), so that the natural approach is to consider it as a hierarchy of processes each with wide-range scaling, i.e., each with nonlinear mechanisms that repeat scale after scale over potentially wide ranges. Following the works of *Lovejoy and Schertzer* [1986], *Schmitt et al.* [1995], *Pelletier* [1998], *Koscielny-Bunde et al.* [1998], *Talkner and Weber* [2000], *Blender and Fraedrich* [2003], *Ashkenazy et al.* [2003], *Huybers and Curry* [2006], and *Rybski et al.* [2008], this approach is increasingly superseding earlier approaches that postulated more or less white noise backgrounds with a large number of spectral "spikes" corresponding to many different quasiperiodic processes. This includes the slightly more sophisticated variants

[e.g., *Mitchell*, 1976], which retain the spikes but replace the white noise with a hierarchy of Ornstein-Uhlenbeck processes (white noises and their integrals). In the spectrum, these appear as "spikes" and "shelves" (see also *Fraedrich et al.* [2009] for a hybrid, which includes a single (short) scaling regime).

Over the past 25 years, scaling approaches have also been frequently applied to the atmosphere, mostly at small or regional scales but, in the last 5 years, increasingly to global scales. This has given rise to a new scaling synthesis covering the entire gamut of meteorological scales from milliseconds to beyond the $\approx$10 day period, which is the typical lifetime of planetary structures, i.e., the weather regime. In the *Lovejoy and Schertzer* [2010] review, it was concluded that the theory and data were consistent with wide range but anisotropic spatial scaling and that the lifetime of planetary-sized structures provides the natural scale at which to distinguish weather and a qualitatively different lower-frequency regime. Figure 1a shows a recent composite indicating the three basic regimes covering the range of time scales from $\approx$100 kyr down to weather scales.

The label "weather" for the high-frequency regime seems clearly justified and requires no further comment. Similarly the lowest frequencies correspond to our usual ideas of
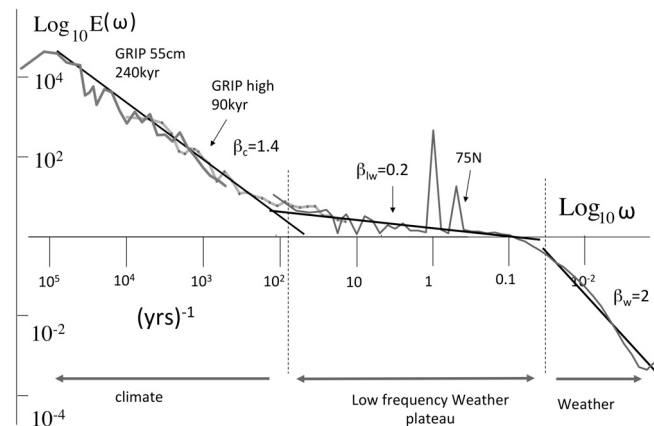
Figure 1a. A modern composite based only on two sources: the Greenland Ice Core Project (GRIP) core (paleotemperatures from Summit Greenland) and the Twentieth Century Reanalyses (20CR) at the same latitude (75°N, thin line on the right). All spectra have been averaged over logarithmically spaced bins, 10 per order of magnitude, and the 20CR spectra have been averaged over all 180° longitude, 2° × 2° elements; frequency units are (years)$^{-1}$. The thin gray line with points is the mean of the GRIP 5.2 resolution data for the last 90 kyr, and the (lowest) frequency line is from the lower-resolution (55 cm) GRIP core interpolated to 200 year resolution and going back 240 kyr. The black reference lines have absolute slopes $\beta_{lw} = 0.2$, $\beta_c = 1.4$, and $\beta_w = 2$ as indicated. The arrows at the bottom indicate the basic qualitatively different scaling regimes.

multidecadal, multicentennial, multimillennial variability as "climate." However, labeling the intermediate region "low-frequency weather" (rather than say "high-frequency climate") needs some justification. The point is perhaps made more clearly with the help of Figure 1b, which shows a blowup of Figure 1a with both globally and locally averaged instrumentally based spectra as well as the spectrum of the output of the stochastic fractionally integrated flux (FIF) model [*Schertzer and Lovejoy*, 1987] and the spectrum of the output of a standard global climate model (GCM) "control run," i.e., without special anthropogenic, solar, volcanic, orbital, or other climate forcings. This regime is, therefore, no more than "low-frequency weather"; it contains no new inter-
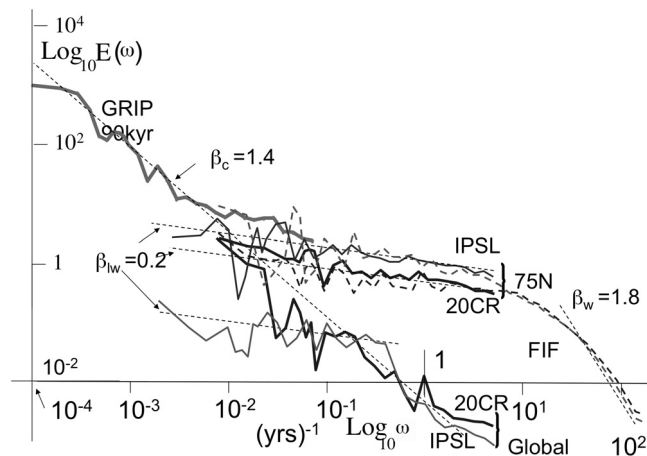
Figure 1b. A comparison of the spectra of temperature fluctuations from the GRIP Greenland Summit core, last 90 kyr, 5.2 year resolution (thick gray, upper left), monthly 20CR reanalysis (black), global (bottom) and 2° resolution (top at 75°N), and a 500 year control run of the monthly Institut Pierre Simon Laplace (IPSL) GCM (gray) used in the 4th IPCC report, at the corresponding resolutions. Frequency units are (years)$^{-1}$. The dashed lines are the detrended daily, grid-scale data (75°N 20CR, dashed dark) and the cascade-based fractionally integrated flux (FIF) simulation (dashed light), both adjusted vertically to coincide with the analyses of the other, monthly scale data. Reference lines with slopes $\beta_c = 1.4$, $\beta_{lw} = 0.2$, $\beta_w = 1.8$ are shown. Notice that the IPSL control run, which lacks external climate forcing and is therefore simply low-frequency weather as well as the low-frequency extension of the cascade-based FIF model, continues to have shallow spectral slopes out to their low-frequency limits, whereas the globally averaged 20CR and paleospectra follow $\beta_c \approx 1.4$ to roughly follow their low-frequency limits. Hence, the plateau is best considered "low-frequency weather": the true climate regime has a much steeper spectrum determined either by new low-frequency internal interactions or by the low-frequency climate "forcing" (solar, orbital, volcanic, anthropogenic, or other); Figure 1a shows that the $\beta_c \approx 1.4$ regime continues to $\approx(100 \text{ kyr})^{-1}$.

nal dynamical elements or any new forcing mechanism. As we discuss below, whereas the spectra from data (especially when globally averaged) begin to rise for frequencies below $\approx(10 \text{ years})^{-1}$, both the FIF and GCM control runs maintain their gently sloping "plateau-like" behaviors out to at least $(500 \text{ years})^{-1}$ (note that we shall see that the "plateau" is not perfectly flat, but its logarithmic slope is small, typically in the range -0.2 to -0.6). Similar conclusions for the control runs of other GCMs at even lower frequencies were found by *Blender et al.* [2006] and *Rybski et al.* [2008] so that it seems that in the absence of external climate forcings, the GCMs reproduce the low-frequency weather regime but not the lower-frequency strongly spectrally rising regime that requires some new *climate* ingredient. The aim of this chapter is to understand the natural variability so that the important question of whether or not GCMs with realistic forcings might be able to reproduce the low-frequency climate regime is outside our present scope. Certainly, existing studies of the scaling of forced GCMs [*Vyushin et al.*, 2004; *Blender et al.*, 2006; *Rybski et al.*, 2008] have consistently reported unique low-frequency weather, but not climate, exponents, and this even at the lowest-simulated frequencies.

2. TEMPORAL SCALING, WEATHER, LOW-FREQUENCY WEATHER, AND THE CLIMATE

2.1. Discussion

Although spatial scaling is fundamental for weather processes, time scales much greater than $\tau_w \approx 10$ days the spatial degrees of freedom essentially collapse (via a "dimensional transition," section 2.5), so that we focus only on temporal variability. Indeed, *Lovejoy and Schertzer* [2012] argue that the spatial variability in the low-frequency weather regime is very large and is associated with different climatic zones. However, it is primarily due to even lower frequency climate-scale processes, so we do not pursue it here.

In order to simplify things as much as possible in section 2, we will only use spectra. Consider a random field $f(t)$ where t is time. Its "spectral density" $E(\omega)$ is the average total contribution to the variance of the process due to structures with frequency between ω and $\omega + d\omega$ (i.e., due to structures of duration $\tau = 2\pi/\omega$, where τ is the corresponding time scale). $E(\omega)$ is thus defined as

$$E(\omega) = \langle |\widetilde{f(\omega)}|^2 \rangle, \tag{1}$$

where $\widetilde{f(\omega)}$ is the Fourier transform of $f(t)$, and the angular brackets indicate statistical averaging. Here $\langle f(t)^2 \rangle$ is thus the total variance (assumed to be independent of time), so that the spectral density thus satisfies $\langle f(t)^2 \rangle = \int_0^\infty E(\omega)d\omega$.

In a scaling regime, we have power law spectra:

$$E(\omega) \approx \omega^{-\beta}. \tag{2}$$

If the time scales are reduced in scale by factor λ, we obtain $t \to \lambda^{-1}t$; this corresponds to a "blow up" in frequencies: $\omega \to \lambda\omega$; and the power law $E(\omega)$ (equation (2)) maintains its form: $E \to \lambda^{-\beta}E$ so that E is "scaling," and the spectral exponent β is "scale invariant." Thus, if empirically we find E to be of the form equation (2), we take this as evidence for the scaling of the field f. Note that numerical spectra have well-known finite size effects; the low-frequency effects have been dealt with below using standard "windowing" techniques (here a Hann window was used to reduce spectral leakage).

2.2. Temporal Spectral Scaling in the Weather Regime

One of the earliest atmospheric spectral analyses was that of the work of *Van der Hoven* [1957], whose graph is at the origin of the legendary "mesoscale gap," the supposedly energy-poor spectral region between roughly 10–20 min and ≈4 days (ignoring the diurnal spike). Even until fairly recently, textbooks regularly reproduced the spectrum (often redrawing it on different axes or introducing other adaptations), citing it as convincing empirical justification for the neat separation between low-frequency isotropic 2-D turbulence, identified with the weather, and high-frequency isotropic 3-D "turbulence." This picture was seductive since if the gap had been real, the 3-D turbulence would be no more than an annoying source of perturbation to the (2-D) weather processes.

However, it was quickly and strongly criticized (e.g., by *Goldman* [1968], *Pinus* [1968], *Vinnichenko* [1969], *Vinnichenko and Dutton* [1969], *Robinson* [1971], and indirectly by *Hwang* [1970]). For instance, on the basis of much more extensive measurements, *Vinnichenko* [1969] commented that even if the mesoscale gap really existed, it could only be for less than 5% of the time; he then went on to note that Van der Hoven's spectrum was actually the superposition of four spectra and that the extreme set of high-frequency measurements were taken during a single 1 h long period during an episode of "near-hurricane" conditions, and these were entirely responsible for the high-frequency "bump."

More modern temporal spectra are compatible with scaling from dissipation scales to ≈5–20 days. Numerous wind and temperature spectra now exist from milliseconds to hours and days showing, for example, that $\beta \approx 1.6$ and 1.8 for v and T, respectively; some of this evidence is reviewed by *Lovejoy and Schertzer* [2010, 2012]. Figure 2 shows an example of the hourly temperature spectrum for frequencies down to (4 years)$^{-1}$. According to Figure 2, it is plausible that the
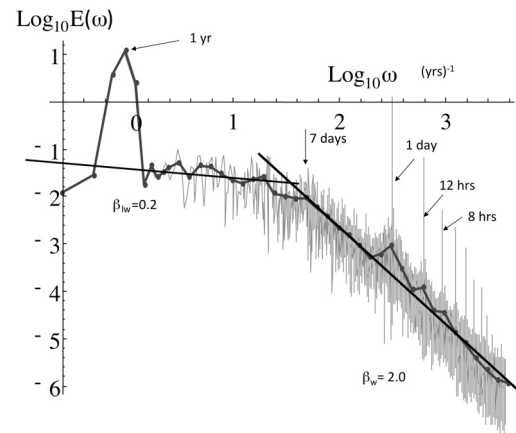
Figure 2. Scaling of hourly surface temperatures from four stations in the northwest United States for 4 years (2005–2008), taken from the U.S. Climate Reference Network. One can see that in spite of the strong diurnal cycle (and harmonics), the basic scaling extends to about 7 days. The reference lines (with absolute slopes 0.2, 2) are theoretically motivated for low-frequency weather and weather scales, respectively. The spectra of hourly surface temperature data are from four nearly colinear stations running northwest-southeast in the United States (Lander, Wyoming; Harrison, Nebraska; Whitman, Nebraska; and Lincoln, Nebraska. The gray line is the raw spectrum; the thick line is the spectrum of the periodically detrended spectrum, averaged over logarithmically spaced bins, 10 per order of magnitude.

scaling in the temperature holds from small scales out to scales of ≈5–10 days, where we see a transition. This transition is essentially the same as the low-frequency "bump" observed by Van der Hoven; its appearance only differs because he used a $\omega E(\omega)$ rather than $\log E(\omega)$ plot.

2.3. Temporal Spectral Scaling in the Low-Frequency Weather-Climate Regime

Except for the annual cycle, the roughly flat low-frequency spectral transitions in Figure 2 (and Figure 1a between ≈10 days and 10 years) are qualitatively reproduced in all the standard meteorological fields, and the transition scale τ_w is relatively constant. Figure 3 shows estimates of τ_w, estimated using reanalyses taken from the Twentieth Century Reanalysis project (20CR) [*Compo et al.*, 2011] on 2° × 2° grid boxes. Also shown are estimates of τ_c, the scale where the latter ends and the climate regime begins. Between τ_w and τ_c is the low-frequency weather regime; it covers a range of a factor ≈1000 in scale. Also shown are estimates of the planetary-scale eddy turnover time discussed below.

Figure 4 shows the surface air temperature analysis out to lower frequencies and compares this with the corresponding spectrum for sea surface temperatures (SSTs) (section 2.7). We see that the ocean behavior is qualitatively similar except
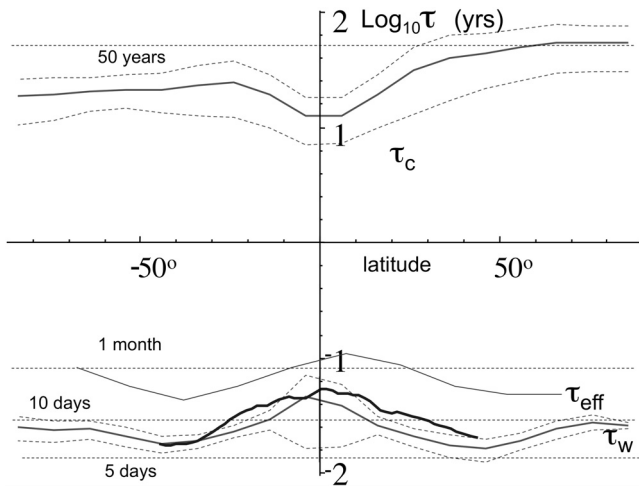
Figure 3. Variation of (bottom) τ_w and (top) τ_c as a function of latitude as estimated from the 138 year long 20CR reanalyses, 700 mb temperature field, compared with (bottom) the theoretically predicted planetary-scale eddy turnover time (τ_{eddy}, black) and the effective external scale (τ_{eff}) of the temperature cascade estimated from the European Centre for Medium-Range Weather Forecasts interim reanalysis for 2006 (thin gray). The τ_w estimates were made by performing bilinear log-log regressions on spectra from 180 day long segments averaged over 280 segments per grid point. The thick gray curves show the mean over all the longitudes; the dashed lines are the corresponding longitude to longitude 1 standard deviation spreads. The τ_c were estimated by bilinear log-log fits on the Haar structure functions applied to the same data but averaged monthly.

that the transition time scale τ_o is ≈ 1 year, and the "low-frequency ocean" exponent $\beta_{lo} \approx 0.6$ is a bit larger than the corresponding $\beta_{lw} \approx 0.2$ for the air temperatures ("*lw*," "*lo*" for "low" frequency "weather" and "ocean," respectively). For comparison, we also show the best fitting Orenstein-Uhlenbeck processes (essentially integrals of white noises, i.e., with $\beta_w = 2$, $\beta_{lw} = 0$); these are the basis of stochastic linear modeling approaches [e.g., *Penland*, 1996]. We see that they are only rough approximations to the true spectra.

To underline the ubiquity of the low-frequency weather regime, its low β character, and to distinguish it from the higher-frequency weather regime, this regime was called the "spectral plateau" [*Lovejoy and Schertzer*, 1986], although it is somewhat of a misnomer since it is clear that the regime has a small but nonzero logarithmic slope whose negative value we indicate by β_{lw}. The transition scale τ_w was also identified as a weather scale by *Koscielny-Bunde et al.* [1998].

2.4. The Weather Regime, Space-Time Scaling, and Some Turbulence Theory

In order to understand the weather and low-frequency weather scaling, we briefly recall some turbulence theory

using the example of the horizontal wind v. In stratified scaling turbulence (the 23/9D model) [*Schertzer and Lovejoy*, 1985a; *Schertzer et al.*, 2012], the energy flux ε dominates the horizontal, and the buoyancy variance flux ϕ dominates the vertical so that horizontal wind fluctuations Δv (e.g., differences, see section 3) follow

$$\Delta v(\Delta x) = \varepsilon^{1/3}\Delta x^{H_h}, \quad H_h = 1/3, \tag{3a}$$

$$\Delta v(\Delta y) = \varepsilon^{1/3}\Delta y^{H_h}, \quad H_h = 1/3, \tag{3b}$$

$$\Delta v(\Delta z) = \phi^{1/5}\Delta z^{H_v}, \quad H_v = 3/5, \tag{3c}$$

$$\Delta v(\Delta t) = \varepsilon^{1/2}\Delta t^{H_\tau}, \quad H_\tau = 1/2, \tag{3d}$$
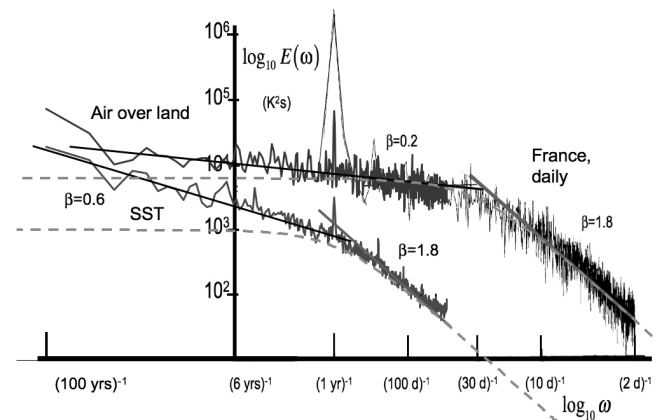
Figure 4. Superposition of the ocean and atmospheric plateaus showing their great qualitative similarity. (bottom left) A comparison of the monthly SST spectrum) and (top) monthly atmospheric temperatures over land for monthly temperature series from 1911 to 2010 on a $5° \times 5°$ grid (the NOAA National Climatic Data Center data). Only those near complete series (missing less than 20 months out of 1200) were considered; there were 465 for the SST and 319 for the land series; the missing data were filled using interpolation. The reference slopes correspond to (top) $\beta = 0.2$, (bottom left) 0.6, and (bottom right) 1.8. A transition at 1 year corresponds to a mean ocean $\varepsilon_o \approx 1 \times 10^{-8}$ m^2 s^{-3}. The dashed lines are Orenstein-Uhlenbeck processes (of the form $E(\omega) = \sigma^2/(\omega^2 + a^2)$, where σ and a are constants) used as the basis for stochastic linear forcing models. (right) The average of five spectra from 6 year long sections of a 30 year series of daily temperatures at a station in France (black) (taken from the work of *Lovejoy and Schertzer* [1986]). The gray reference line has a slope 1.8. The relative up-down placement of this daily spectrum with the monthly spectra (corresponding to a constant factor) was determined by aligning the atmospheric spectral plateaus (i.e., the black and gray spectra). The raw spectra are shown (no averaging over logarithmically spaced bins).

where Δx, Δy, Δz, Δt are the increments in horizontal coordinates, vertical coordinate, and time, respectively, and the exponents H_h, H_v, H_τ are "fluctuation" or "nonconservation" exponents in the horizontal, vertical, and time, respectively. Since the mean fluxes are independent of scale (i.e., $\langle \varepsilon \rangle$, $\langle \phi \rangle$ are constant, angular brackets indicate ensemble averaging), these exponents express how the mean fluctuations Δv increase ($H > 0$) or decrease ($H < 0$) with the scale (e.g., the increments, when $H > 0$, see below). Equations (3a) and (3b) describe the real space horizontal [*Kolmogorov*, 1941] scaling, and equation (3c) describes the vertical Bolgiano-Obukhov [*Bolgiano*, 1959; *Obukhov*, 1959] scaling for the velocity. The anisotropic Corrsin-Obukov law for passive scalar advection is obtained by the replacements $v \rightarrow \rho$; $\varepsilon \rightarrow \chi^{3/2}\varepsilon^{-1/2}$, where ρ is the passive scalar density, χ is the passive scalar variance flux [*Corrsin*, 1951; *Obukhov*, 1949].

Before proceeding, here are a few technical comments. In equation (3), the equality signs should be understood in the sense that each side of the equation has the same scaling properties: the FIF model (Figure 1b) is essentially a more precise interpretation of the equations in terms of fractional integrals of order H. Ignoring intermittency (associated with multifractal fluxes, which we discuss only briefly below), the spectral exponents are related to H as $\beta = 1 + 2H$ so that $\beta_h = 5/3$, $\beta_v = 11/5$, $\beta_\tau = 2$. Finally, although the notation "H" is used in honor of E. Hurst, in multifractal processes, it is generally *not* identical to the Hurst (i.e., rescaled range, "R/S") exponent, the relationship between the two is nontrivial.

Although these equations originated in classical turbulence theory, the latter were all spatially statistically isotropic so that the simultaneous combination of the horizontal laws (3a) and (3b) with the vertical law (3c) is nonclassical. Since the isotropy assumption is very demanding, the pioneers originally believed that the classical laws would hold over only scales of scales of hundreds of meters. The anisotropic extension implied by equations (3a)–(3d) is itself based on a generalization of the notion of scale invariance and thus has the effect of radically changing the potential range of validity of the laws. For example, even the finite thickness of the troposphere, which in isotropic turbulence would imply a scale break at around 10 km, no longer implies a break in the scaling. Beginning with the work of *Schertzer and Lovejoy* [1985b], it has been argued that atmospheric variables including the wind do indeed have wide range (anisotropic) scaling statistics (see the review by *Lovejoy and Schertzer* [2010]).

In addition, the classical turbulence theories were for spatially uniform ("homogeneous") turbulence in which the fluxes were quasiconstant (e.g., with Gaussian statistics). In order for these laws to apply up to planetary scales, starting in the 1980s [*Parisi and Frisch*, 1985;

Schertzer and Lovejoy, 1985b], they were generalized to strongly variable (intermittent) multiplicative cascade processes yielding multifractal fluxes so that, although the mean flux statistics $\langle \varepsilon_{\Delta x} \rangle$ remain independent of scale Δx, the statistical moments:

$$\langle \varepsilon_{\Delta x}{}^q \rangle \approx \Delta x^{-K(q)}, \qquad (4)$$

where $\varepsilon_{\Delta x}$ is the flux averaged over scales Δx, and $K(q)$ is the (convex) moment scaling exponent. Although $K(1) = 0$, for $q \neq 1$, $K(1) \neq 0$ so that $\langle \varepsilon_{\Delta x}{}^q \rangle$ is strongly scale *dependent*, the fluxes are thus the densities of singular multifractal measures.

Along with the spatial laws (equations (3a)–(3c)), we have included equation (3d), which is the result for the pure time evolution in the absence of an overall advection velocity; this is the classical Lagrangian version of the Kolmogorov law [*Inoue*, 1951; *Landau and Lifschitz*, 1959]; it is essentially the result of dimensional analysis using ε and Δt rather than ε and Δx. Although Lagrangian statistics are notoriously difficult to obtain empirically (see, however, *Seuront et al.* [1996]), they are roughly known from experience and are used as the basis for the space-time or "Stommel" diagrams that adorn introductory meteorology textbooks (see *Schertzer et al.* [1997] and *Lovejoy et al.* [2000] for scaling adaptations).

Due to the fact that the wind is responsible for advection, the spatial scaling of the horizontal wind leads to the temporal scaling of all the fields. Unfortunately, space-time scaling is somewhat more complicated than pure spatial scaling. This is because, at meteorological time scales, we must take into account the mean advection of structures and the Galilean invariance of the dynamics. The effect of the Galilean invariance/advection of structures is that the temporal exponents in the Eulerian (fixed Earth) frame become the same as in the horizontal direction (i.e., in (x,y,t) space, we have "trivial anisotropy," i.e., with "effective" temporal exponent $H_{\tau\mathrm{eff}} = H_h$) [*Lovejoy et al.*, 2008; *Radkevitch et al.*, 2008]. At the longer time scales of low-frequency weather, the scaling is broken because the finite size of the Earth implies a characteristic lifetime ("eddy turnover time") of planetary-scale structures. Using equations (3a) and (3b) with $\Delta x = L_e$, we obtain: $\tau_{\mathrm{eddy}} = L_e/\Delta v(L_e) = \varepsilon_w{}^{-1/3}L_e{}^{2/3}$, where $L_e = 20,000$ km, the size of the planet, and ε_w is the globally averaged energy flux density.

Considering time scales longer than τ_{eddy}, the effect of the finite planetary size implies that the spatial degrees of freedom become ineffective (there is a "dimensional transition") so that instead of interactions in (x,y,z,t) space for long times, the interactions are effectively only in t space, and this implies a drastic change in the statistics, summarized in the next section.

2.5. Low-Frequency Weather and the Dimensional Transition

To obtain theoretical predictions for the statistics of atmospheric variability at time scales $\tau > \tau_w$ (i.e., in the low-frequency weather regime), we can take the FIF [*Schertzer and Lovejoy*, 1987] model that produces multifractal fields respecting equation (3) and extend it to processes with outer time scales $\tau_c \gg \tau_w$. The theoretical details are given by *Lovejoy and Schertzer* [2010, 2012], but the upshot of this is that we expect the energy flux density ε to factor into a statistically independent space-time weather process $\varepsilon_w(\underline{r},t)$ and a low-frequency weather process $\varepsilon_{lw}(t)$, which is only dependent on time:

$$\varepsilon(\underline{r},t) = \varepsilon_w(\underline{r},t)\varepsilon_{lw}(t). \tag{5}$$

In this way, the low-frequency energy flux $\varepsilon_{lw}(t)$, which physically is the result of nonlinear radiation/cloud interactions, multiplicatively modulates the high-frequency space-time weather processes. *Lovejoy and Schertzer* [2012] discuss extensions of this model to include even lower frequency space-time climate processes; it is sufficient to include a further climate flux factor in equation (5).

The theoretical statistical behavior of $\varepsilon_{lw}(t)$ is quite complex to analyze and has some surprising properties. Some important characteristics are the following: (1) At large temporal lags Δt, the autocorrelation $\langle \varepsilon_{lw}(t)\,\varepsilon_{lw}(t - \Delta t) \rangle$ ultimately decays as Δt^{-1}, although very large ranges of scale may be necessary to observe it. (2) Since the spectrum is the Fourier transform of the autocorrelation, and the transform of a pure Δt^{-1} function has a low- (and high) frequency divergence, the actual spectrum of the low-frequency weather regime depends on its overall range of scales $\Lambda_c = \tau_c/\tau_w$. From Figure 3, we find that to within a factor of ≈ 2, the mean Λ_c over the latitudes is ≈ 1100. (3) Over surprisingly wide ranges (factors of 100–1000 in frequency for values of Λ_c in the range 2^{10}–2^{16}), one finds "pseudoscaling" with nearly constant spectral exponents β_{lw}, which are typically in the range 0.2–0.4. (4) The statistics are independent of H and only weakly dependent on $K(q)$.

In summary, we therefore find for the overall weather/low-frequency weather (FIF) model

$$\begin{aligned} E(k) &\approx k^{-\beta_w}; & k &> L_e^{-1} \\ E(\omega) &\approx \omega^{-\beta_w}; & \omega &> \tau_w^{-1}, \\ E(\omega) &\approx \omega^{-\beta_{lw}}; & \tau_c^{-1} &< \omega < \tau_w^{-1}, \end{aligned} \tag{6}$$

where k is the modulus of the horizontal wave vector, τ_c is the long external climate scale where the low-frequency weather regime ends (see discussion below), and β_l, β_{lw} are

$$\begin{aligned} \beta_w &= 1 + 2H_w - K(2) \\ 0.2 &< \beta_{lw} < 0.6. \end{aligned} \tag{7}$$

In the low-frequency weather regime, the intermittency (characterized by $K(q)$) decreases as we average the process over scales $> \tau_w$ so that the low-frequency weather regime has an effective fluctuation exponent H_{lw}:

$$H_{lw} \approx -(1 - \beta_{lw})/2. \tag{8}$$

The high-frequency weather spectral exponents β_w, H_w are the usual ones, but the low-frequency weather exponents β_{lw}, H_{lw} are new. Since $\beta_{lw} < 1$, we have $H_{lw} < 0$, and using $0.2 < \beta_{lw} < 0.6$ corresponding to $-0.4 < H_{lw} < -0.2$, this result already explains the preponderance of spectral plateau β around that value already noted. However, as we saw in Figure 4, the low-frequency ocean regime has a somewhat high value $\beta_{oc} \approx 0.6$, $H_{oc} \approx -0.2$; *Lovejoy and Schertzer* [2012] use a simple coupled ocean-atmosphere model to show how this could arise as a consequence of double (atmosphere and ocean) dimensional transitions. The fact that $H_{lw} < 0$ indicates that the mean fluctuations decrease with scale so that the low-frequency weather and ocean regimes are "stable."

2.6. The Transition Time Scale From Weather to Low-Frequency Weather Using "First Principles"

Figures 1–4 show evidence that temporal scaling holds from small scales to a transition scale τ_w of around 5–20 days, which we mentioned was the eddy turnover time (lifetime) of planetary-scale structures. Let us now consider the physical origin of this scale in more detail. In the famous [*Van der Hoven*, 1957] $\omega E(\omega)$ versus $\log\omega$ plot, its origin was argued to be due to "migratory pressure systems of synoptic weather-map scale." The corresponding features at around 4–20 days notably for temperature and pressure spectra were termed "synoptic maxima" by *Kolesnikov and Monin* [1965] and *Panofsky* [1969] in reference to the similar idea that it was associated with synoptic-scale weather dynamics (see *Monin and Yaglom* [1975] for some other early references).

More recently, *Vallis* [2010] suggested that τ_w is the basic lifetime of baroclinic instabilities, which he estimated using the inverse Eady growth rate: $\tau_{\text{Eady}} \approx L_d/U$, where the deformation rate is $L_d = NH/f_0$, f_0 is the Coriolis parameter, and H is the thickness of the troposphere, where N is the mean Brunt-Väisällä frequency, and U is the typical wind. The Eady growth rate is obtained by linearizing the equations about a hypothetical state with both uniform shear and stratification across the troposphere. By taking $H \approx 10^4$ m, $f_0 \approx 10^{-4}$ s^{-1}, $N = 0.01$ Hz, and $U \approx 10$ m s^{-1}, Vallis

obtained the estimate $L_d \approx 1000$ km. Using the maximum Eady growth rate theoretically introduces a numerical factor 3.3 so that the actual predicted inverse growth rate is: $3.3\tau_{\mathrm{Eady}} \approx 4$ days. Vallis similarly argued that this also applies to the oceans but with $U \approx 10$ cm s^{-1} and $L_d \approx 100$ km yielding $3.3\tau_{\mathrm{Eady}} \approx 40$ days. The obvious theoretical problem with using τ_{Eady} to estimate τ_w is that the former is expected to be valid in homogeneous, quasilinear systems, whereas the atmosphere is highly heterogeneous with vertical and horizontal structures (including strongly nonlinear cascade structures) extending throughout the troposphere to scales substantially larger than L_d. Another difficulty is that although the observed transition scale τ_w is well behaved at the equator (Figure 3), f_0 vanishes implying that L_d and τ_{Eady} diverge: using τ_{Eady} as an estimate of τ_w is at best a midlatitude approximation. Finally, there is no evidence for any special behavior at length scales near $L_d \approx 1000$ km.

If there is (at least statistically) a well-defined relation between spatial scales and lifetimes (the "eddy turnover time"), then the lifetime of planetary-scale structures τ_{eddy} is of fundamental importance. The shorter period ($\tau < \tau_{\mathrm{eddy}}$) statistics are dominated by structures smaller than planetary size, whereas for $\tau > \tau_{\mathrm{eddy}}$, they are dominated by the statistics of many lifetimes of planetary-scale structures. It is therefore natural to take $\tau_w \approx \tau_{\mathrm{eddy}} = \varepsilon_w^{-1/3} L_e^{2/3}$.

In order to estimate τ_w, we therefore need an estimate of the globally averaged flux energy density ε_w. We can estimate ε_w by using the fact that the mean solar flux absorbed by the Earth is ≈ 200 W m^{-2} [e.g., *Monin*, 1972]. If we distribute this over the troposphere (thickness $\approx 10^4$ m), with mean air density ≈ 0.75 kg m^{-3}, and we assume a 2% conversion of energy into kinetic energy [*Palmén*, 1959; *Monin*, 1972], then we obtain a value $\varepsilon_w \approx 5 \times 10^{-4}$ m^2 s^{-3}, which is indeed typical of the values measured in small-scale turbulence [*Brunt*, 1939; *Monin*, 1972]. Using the European Centre for Medium-Range Weather Forecasts (ECMWF) interim reanalysis to obtain a modern estimate of ε_w, *Lovejoy and Schertzer* [2010] showed that although ε is larger in midlatitudes than at the equator and that at 300 mb it reaches a maximum, the global tropospheric average is $\approx 10^{-3}$ m^2 s^{-3}. They also showed that the latitudinally varying ε explains to better than ±20% the latitudinal variation of the hemispheric antipodes velocity differences (using $\Delta v = \varepsilon^{1/3} L_e^{1/3}$). They concluded that the solar energy flux does a good job of explaining the horizontal wind fluctuations up to planetary scales. In addition, we can now point to Figure 3, which shows that the latitudinally varying ECMWF estimates of $\varepsilon_w(\theta)$ do indeed lead to $\tau_{\mathrm{eddy}}(\theta)$ very close to the direct 20CR $\tau_w(\theta)$ estimates for the 700 mb temperature field.

2.7. Ocean "Weather" and "Low-Frequency Ocean Weather"

It is well known that for months and longer time scales, ocean variability is important for atmospheric dynamics; before explicitly attempting to extend this model of weather variability beyond τ_w, we must therefore consider the role of the ocean. The ocean and the atmosphere have many similarities; from the preceding discussion, we may expect analogous regimes of "ocean weather" to be followed by an ocean spectral plateau both of which will influence the atmosphere. To make this more plausible, recall that both the atmosphere and ocean are large Reynolds' number turbulent systems and both are highly stratified, albeit due to somewhat different mechanisms. In particular, there is no question that at least over some range, horizontal ocean current spectra are dominated by the ocean energy flux ε_o. It roughly follows that $E(\omega) \approx \omega^{-5/3}$ and presumably in the horizontal: $E(k) \approx k^{-5/3}$ (i.e., $\beta_o = 5/3$, $H_o = 1/3$) [see, e.g., *Grant et al.*, 1962; *Nakajima and Hayakawa*, 1982]. Although surprisingly few current spectra have been published, the recent use of satellite altimeter data to estimate sea surface height (a pressure proxy) has provided relevant empirical evidence that $k^{-5/3}$ continues out to scales of at least hundreds of kilometers, refueling the debate about the spectral exponent and the scaling of the current [see *Le Traon et al.*, 2008].

Although empirically the current spectra (or their proxies) at scales larger than several hundred kilometers are not well known, other spectra, especially those of SSTs, are known to be scaling over wide ranges, and due to their strong nonlinear coupling with the current, they are relevant. Using mostly remotely sensed IR radiances, and starting in the early 1970s, there is much evidence for SST scaling up to thousands of kilometers with $\beta \approx 1.8$–2, i.e., nearly the same as for the atmospheric temperature (see, e.g., *McLeish* [1970], *Saunders* [1972], *Deschamps et al.* [1981, 1984], *Burgert and Hsieh* [1989], *Seuront et al.* [1996], and *Lovejoy et al.* [2000] and a review by *Lovejoy and Schertzer* [2012]).

If, as in the atmosphere, the energy flux dominates the horizontal ocean dynamics, then we can use the same methodology as in the previous subsection (basic turbulence theory (the Kolmogorov law) combined with the mean ocean energy flux ε_o) to predict ocean eddy turnover time and hence the outer scale τ_o of the ocean regime. Thus, for ocean gyres and eddies of size l, we expect there to be a characteristic eddy turnover time (lifetime) $\tau = \varepsilon^{-1/3} l^{2/3}$ with a critical "ocean weather"-"ocean climate" transition time scale obtained when $l = L_e$: $\tau_o = \varepsilon_o^{-1/3} L_e^{2/3}$. Again, we expect a fundamental difference in the statistics for fluctuations of duration $\tau < \tau_o$, the ocean equivalent of "weather" with a turbulent spectrum with roughly $\beta_o \approx 5/3$ (at least for the

current), and for durations $\tau > \tau_o$, the ocean "climate" with a shallow ocean spectral regime with $\beta \approx {<}1$. Since the spatial β for temperature in the atmosphere and ocean are very close, if the β for the current and wind are also close, then so will the β for the temporal temperature spectra.

In order to test this idea, we need the globally averaged ocean current energy flux, ε_o. As expected, ε_o is highly intermittent [see *Robert*, 1976; *Clayson and Kantha*, 1999; *Moum et al.*, 1995; *Lien and D'Asaro*, 2006; *Matsuno et al.*, 2006], and as far as we know, the only attempt to estimate its global average was *Lovejoy and Schertzer* [2012], who used ocean drifter maps of eddy kinetic energy. They found that $\varepsilon_o \approx 10^{-8} \text{ m}^2 \text{ s}^{-3}$ is a reasonable global estimate for the surface layer (it decreases quite rapidly with depth). Using the formula $\tau_o = \varepsilon_o^{-1/3} L_e^{2/3}$ and ε_o in the range 1×10^{-8} to $8 \times 10^{-8} \text{ m}^2 \text{ s}^{-3}$, we find $\tau_o \approx 1$–2 years; compare this with the values for the atmosphere: $\varepsilon_w \approx 10^{-3} \text{ m}^2 \text{ s}^{-3}$, $\tau_w \approx 10$ days.

This provides us with a prediction for the SST spectrum: $E(\omega) \approx \omega^{-1.8}$ for ω $(1 \text{ year})^{-1}$ followed by a transition to a much flatter plateau (here $\approx \omega^{-0.6}$) for the lower frequencies (see Figure 4, which compares the ocean and air over land spectra). While the latter spectrum is, as expected, essentially a pure spectral plateau (with $\beta_{lw} \approx 0.2$, the value cited earlier), we see that the SST spectrum is essentially the same ($\beta_o \approx \beta_w \approx 1.8$) except that $\beta_{lo} \approx 0.6$ and $\tau_o \approx 1$ year. This basic "crossover" to an exponent $\beta_{lo} \approx 0.6$ was already noted by *Monetti et al.* [2003], who estimated it as 300 days. Note also the rough convergence of the spectra at about 100 years, which implies that the land and ocean variability become equal and also the hint that there is a low-frequency rise in the land spectrum for periods $> \approx 30$ years.

2.8. Other Evidence for the Spectral Plateau

Various published scaling composites such as Figures 1a and 1b give estimates for the low-frequency weather exponent β_{lw}, the climate exponent β_c, and the transition scale τ_c; they agree on the basic picture while proposing somewhat different parameter values and transition scales τ_c. For example, *Huybers and Curry* [2006] studied many paleoclimate series as well as the 60 year long National Centers for Environmental Prediction (NCEP) reanalyses concluded that for periods of months up to about 50 years, the spectra are scaling with midlatitude β_{lw} larger than the tropical β_{lw} (their values are 0.37 ± 0.05, 0.56 ± 0.08). Many analyses in the spectral plateau regime have been carried out using in situ data with the detrended fluctuation analysis (DFA) method [*Fraedrich and Blender*, 2003; *Koscielny-Bunde et al.*, 1998; *Bunde et al.*, 2004], SSTs [*Monetti et al.*, 2003], and ≈ 1000 year long Northern Hemisphere reconstructions [*Rybski et al.*, 2006];

see also the works of *Lennartz and Bunde* [2009] and *Lanfredi et al.* [2009] and see the work of *Eichner et al.* [2003], for a review of many scaling analyses and their implications for long-term persistence/memory issue. From the station analyses, the basic conclusions of *Fraedrich and Blender* [2003] were that over land, $\beta \approx 0$–0.1, whereas over the ocean, $\beta \approx 0.3$; *Eichner et al.* [2003] found $\beta \approx 0.3$ over land and using NCEP reanalyses; *Huybers and Curry* [2006] found slightly higher values and noted an additional latitudinal effect (β is higher at the equator). At longer scales, *Blender et al.* [2006] analyzed the anomalous Holocene Greenland paleotemperatures finding $\beta \approx 0.5$ (see section 4.2). Other pertinent analyses are of global climate model outputs and historical reconstructions of the Northern Hemisphere temperatures; these are discussed in detail in section 4.3. Our basic empirical conclusions, in accord with a growing literature, particularly with respect to the temperature statistics, are that β is mostly in the range 0.2–0.4 over land and ≈ 0.6 over the ocean.

3. CLIMATE CHANGE

3.1. What Is Climate Change?

We briefly surveyed the weather scaling, focusing on the transition to the low-frequency weather regime for time scales longer than the lifetimes of planetary-scale eddies, $\tau_w \approx 5$–20 days. This picture was complicated somewhat by the qualitatively similar (and nonlinearly coupled) transition from the analogous ocean "weather" to "low-frequency ocean weather" at $\tau_o \approx 1$ year. Using purely spectral analyses, we found that these low-frequency regimes continued until scales of the order of $\tau_c \approx 10$–100 years, after which the spectra started to steeply rise, marking the beginning of the true climate regime. While the high-frequency regime clearly corresponds to "weather," we termed the intermediate regime "low-frequency weather" since its statistics are not only well reproduced with (unforced) "control" runs of GCMs (Figure 1b) but also by (stochastic, turbulent) cascade models of the weather when these are extended to low frequencies. The term "climate regime" was thus reserved for the long times $\tau > \tau_c$, where the low-frequency weather regime gives way to a qualitatively different and much more variable regime. The new climate regime is thus driven either by new (internal) low-frequency nonlinear interactions or by appropriate low-frequency solar, volcanic, anthropogenic, or eventually orbital forcing at scales $\tau > \tau_c$.

This three-scale-range scaling picture of atmospheric variability leads to a clarification of the rough idea that the climate is nothing more than long-term averages of the

weather. It allows us to precisely define a *climate state* as the average of the weather over the entire low-frequency weather regime up to τ_c (i.e., up to decadal or centennial scales). This paves the way for a straightforward definition of climate *change* as the long-term *changes* in this climate state, i.e., of the statistics of these climate states at scales $\tau > \tau_c$.

3.2. What Is τ_c?

In Figures 1a and 1b, we gave some evidence that τ_c was in the range $(10 \text{ years})^{-1}$ to $(100 \text{ years})^{-1}$; that is, it was near the extreme low-frequency limit of instrumental data. We now attempt to determine it more accurately. Up until now, we primarily used spectral analysis since it is a classical, straightforward technique, whose limitations are well known, and it was adequate for the purpose of determining the basic scaling regimes in time and in space. We now focus on the low frequencies corresponding to several years to ≈100 kyr so that it is convenient to study fluctuations in real rather than Fourier space. There are several reasons for this. The first is that we are focusing on the lowest instrumental frequencies, and so spectral analysis provides only a few useful data points; for example, on data 150 years long, the time scales longer than 50 years are characterized only by three discrete frequencies $\omega = 1, 2, 3$; Fourier methods are "coarse" at low frequencies. The second is that in order to extend the analysis to lower frequencies, it is imperative to use proxies, and these need calibration: the mean absolute amplitudes of fluctuations at a given scale enable us to perform a statistical calibration. The third is that the absolute amplitudes are also important for gauging the physical interpretation and hence significance of the fluctuations.

3.3. Fluctuations and Structure Functions

The simplest fluctuation is also the oldest, the difference: $(\Delta v(\Delta t))_{\text{diff}} = \Delta v(t + \Delta t) - \Delta v(t)$. According to equation (3), the fluctuations follow:

$$\Delta v = \varphi_{\Delta t} \Delta t^H, \tag{9}$$

where $\varphi_{\Delta t}$ is a resolution Δt turbulent flux. From this, we see that the statistical moments follow:

$$\langle \Delta v(\Delta t)^q \rangle = \langle \varphi_{\Delta t}^q \rangle \Delta t^{qH} \approx \Delta t^{\xi(q)}; \quad \xi(q) = qH - K(q); \tag{10}$$

$\xi(q)$ is the (generalized) structure function exponent, and $K(q)$ is the (multifractal, cascade) intermittency exponent, equation (4). The turbulent flux has the property that it is independent of scale Δt, i.e., the first-order moment $\langle \varphi_{\Delta t} \rangle$ is constant; hence, $K(1) = 0$ and $\xi(1) = H$. The physical significance of H is thus that it determines the rate at which fluctuations grow ($H > 0$) or decrease ($H < 0$) with scale Δt. Since the spectrum is a second-order moment, there is the following useful and simple relation between real space and Fourier space exponents:

$$\beta = 1 + \xi(2) = 1 + 2H - K(2). \tag{11}$$

A problem arises since the mean *difference* cannot decrease with increasing Δt; hence, differences are clearly inappropriate when studying scaling processes with $H < 0$: the differences simply converge to a spurious constant depending on the highest frequencies present in the sample. Similarly, when $H > 1$, fluctuations defined as differences saturate at a large Δt independent value; they depend on the lowest frequencies present in the sample. In both cases, the exponent $\xi(q)$ is no longer correctly estimated. The problem is that we need a definition of fluctuations such that $\Delta v(\Delta t)$ is dominated by frequencies $\approx \Delta t^{-1}$.

The need to more flexibly define fluctuations motivated the development of wavelets [e.g., *Bacry et al.*, 1989; *Mallat and Hwang*, 1992; *Torrence and Compo*, 1998], and the related DFA technique [*Peng et al.*, 1994; *Kantelhardt et al.*, 2001; *Kantelhardt et al.*, 2002] for polynomial and multifractal extensions, respectively. In this context, the classical difference fluctuation is only a special case, the "poor man's wavelet." In the weather regime, most geophysical H parameters are indeed in the range 0 to 1 (see, e.g., the review by *Lovejoy and Schertzer* [2010]) so that fluctuations tend to *increase* with scale, so that this classical difference structure function is generally adequate. However, a prime characteristic of the low-frequency weather regime is precisely that $H < 0$ (section 2.5) so that fluctuations *decrease* rather than increase with scale; hence, for studying this regime, difference fluctuations are inappropriate. To change the range of H over which fluctuations are usefully defined, one changes the shape of the defining wavelet, changing both its real and Fourier space localizations. In the usual wavelet framework, this is done by modifying the wavelet directly, e.g., by choosing the Mexican hat or higher-order derivatives of the Gaussian, etc., or by choosing them to satisfy some special criterion. Following this, the fluctuations are calculated as convolutions with fast Fourier (or equivalent) numerical techniques.

A problem with this usual implementation of wavelets is that not only are the convolutions numerically cumbersome, but the physical interpretation of the fluctuations is lost. In contrast, when $0 < H < 1$, the difference structure function is both simple and gives direct information on the typical difference ($q = 1$) and typical variations around this difference

($q = 2$) and even typical skewness ($q = 3$) or typical Kurtosis ($q = 4$) or, if the probability tail is algebraic, of the divergence of high-order moments of differences. Similarly, when $-1 < H < 0$, one can define the "tendency structure function" (below), which directly quantifies the fluctuation's deviation from zero and whose exponent characterizes the rate at which the deviations decrease when we average to larger and larger scales. These poor man's and tendency fluctuations are also very easy to directly estimate from series with uniformly spaced data and, with straightforward modifications, to irregularly spaced data.

The study of real space fluctuation statistics in the low-frequency weather regime therefore requires a definition of fluctuations valid at least over the range $-1 < H < 1$. Before discussing our choice, the Haar wavelet, let us recall the definitions of the difference and tendency fluctuations; the corresponding structure functions are simply the corresponding qth-order statistical moments. The difference/poor man's fluctuation is thus

$$(\Delta v(\Delta t))_{\mathrm{diff}} \equiv |\delta_{\Delta t} v|; \quad \delta_{\Delta t} v = v(t + \Delta t) - v(t), \qquad (12)$$

where δ is the difference operator. Similarly, the "tendency fluctuation" [*Lovejoy and Schertzer*, 2012] can be defined using the series with overall mean removed: $v'(t) = v(t) - \overline{v(t)}$ with the help of the summation operator s by

$$(\Delta v(\Delta t))_{\mathrm{tend}} = \left|\frac{1}{\Delta t}\delta_{\Delta t} s v'\right|; \quad s v' = \sum_{t' \leq t} v'(t'), \qquad (13)$$

where $(\Delta v(\Delta t))_{\mathrm{tend}}$ has a straightforward interpretation in terms of the mean tendency of the data but is useful only for $-1 < H < 0$. It is also easy to implement: simply remove the *overall* mean and then take the mean over intervals Δt: this is equivalent to taking the mean of the differences of the running sum.

We can now define the Haar fluctuation, which is a special case of the Daubechies family of orthogonal wavelets [see, e.g., *Holschneider*, 1995] (for a recent application, see *Ashok et al.* [2010] and for a comparison with the related DFA technique, see *Koscielny-Bunde et al.* [1998, 2006]). This can be done by

$$(\Delta v(\Delta t))_{\mathrm{Haar}} = \left|\frac{2}{\Delta t}\delta^2_{\Delta t/2} s\right| = \left|\frac{1}{\Delta t}((s(t) + s(t + \Delta t)) - 2s(t + \Delta t/2))\right|$$

$$= \left|\frac{2}{\Delta t}\left[\sum_{t+\Delta t/2 \leq t' \leq t+\Delta t} v(t') - \sum_{t \leq t' \leq t+\Delta t/2} v(t')\right]\right|. \qquad (14)$$

From this, we see that the Haar fluctuation at resolution Δt is simply the first difference of the series degraded to resolution $\Delta t/2$. Although this is still a valid wavelet (but with the extra

normalization factor Δt^{-1}), it is almost trivial to calculate, and (thanks to the summing) the technique is useful for series with $-1 < H < 1$.

For pure scaling functions, the difference ($1 > H > 0$) or tendency ($-1 < H < 0$) structure functions are adequate and have obvious interpretations. The real advantage of the Haar structure function is apparent for functions with two or more scaling regimes, one with $H > 0$, one with $H < 0$. From equation (11), we see that ignoring intermittency, this criterion is the same as $\beta < 1$ or $\beta > 1$; hence (see, e.g., Figure 1a), Haar fluctuations will be useful for the data analyzed, which straddle (either at high or low frequencies) the boundaries of the low-frequency weather regime.

Is it possible to "calibrate" the Haar structure function so that the amplitude of typical fluctuations can still be easily interpreted? To answer this, consider the definition of a "hybrid" fluctuation as the maximum of the difference and tendency fluctuations:

$$(\Delta T)_{\mathrm{hybrid}} = max((\Delta T)_{\mathrm{diff}}, (\Delta T)_{\mathrm{tend}}); \qquad (15)$$

the "hybrid structure function" is thus the maximum of the corresponding difference and tendency structure functions and therefore has a straightforward interpretation. The hybrid fluctuation is useful if a calibration constant C can be found such that

$$\langle \Delta T(\Delta t)^q_{\mathrm{hybrid}}\rangle \approx C^q \langle \Delta T(\Delta t)^q_{\mathrm{Haar}}\rangle. \qquad (16)$$

In a pure scaling process with $-1 < H < 1$, this is clearly possible since the difference or tendency fluctuations yield the same scaling exponent. However, in a case with two or more scaling regimes, this equality cannot be exact, but as we see this in the next section, it can still be quite a reasonable approximation.

3.4. Application of Haar Fluctuations to Global Temperature Series

Now that we have defined the Haar fluctuations and corresponding structure function, we can use them to analyze a fundamental climatological series: the monthly resolution global mean surface temperature. At this resolution, the high-frequency weather variability is largely filtered out, and the statistics are dominated first by the low-frequency weather regime ($H < 0$) and then at low enough frequencies by the climate regime ($H > 0$).

Several such series have been constructed. The three we chose are the NOAA National Climatic Data Center (NCDC) merged land air and SST data set (from 1880 on a $5° \times 5°$ grid) (see *Smith et al.* [2008] for details), the NASA Goddard Institute for Space Studies (GISS) data set (from 1880 on a

$2° \times 2°$) [*Hansen et al.*, 2010], and the HadCRUT3 data set (from 1850 to 2010 on a $5° \times 5°$ grid). HadCRUT3 is a merged product created out of the Climate Research Unit HadSST2 [*Rayner et al.*, 2006] SST data set and its companion data set CRUTEM3 of atmospheric temperatures over land. The NOAA NCDC and NASA GISS are both heavily based on the Global Historical Climatology Network [*Peterson and Vose*, 1997] and have many similarities including the use of sophisticated statistical methods to smooth and reduce noise. In contrast, the HadCRUTM3 data is less processed. Unsurprisingly, these series are quite similar, although analysis of the scale by scale differences between the spectra is interesting [see *Lovejoy and Schertzer*, 2012].

Each grid point in each data set suffered from missing data points so that here we consider the globally averaged series obtained by averaging over all the available data for the common 129 year period 1880–2008. Before analysis, each series was periodically detrended to remove the annual cycle; if this is not done, then the scaling near $\Delta t \approx 1$ year will be artificially degraded. The detrending was done by setting the amplitudes of the Fourier components corresponding to annual periods to the "background" spectral values.

Figure 5 shows the comparison of the difference, tendency, hybrid, and Haar root-mean-square (RMS) structure functions $\langle \Delta T(\Delta t)^2 \rangle^{1/2}$, the latter increased by a factor $C = 10^{0.35} \approx 2.2$. Before commenting on the physical implications, let us first make some technical remarks. It can be seen that the "calibrated" Haar and hybrid structure functions are very close; the deviations are $\pm 14\%$ over the entire range of nearly a factor 10^3 in Δt. This implies that the indicated amplitude scale of the calibrated Haar structure function in degrees K is quite accurate and that to a good approximation, the Haar structure function can preserve the simple interpretation of the difference and tendency structure functions: in regions where the logarithmic slope is between -1 and 0, it approximates the tendency structure function, whereas in regions where the logarithmic slope is between 0 and 1, the calibrated Haar structure function approximates the difference structure function. For example, from the graph, we can see that global-scale temperature fluctuations decrease from ≈ 0.3 K at monthly scales, to ≈ 0.2 K at 10 years and then increase to ≈ 0.8 K at ≈ 100 years. All of the numbers have obvious implications, although note that they indicate the mean overall range of the fluctuations so that, for example, the 0.8 K corresponds to ± 0.4 K, etc.

From Figure 5, we also see that the global surface temperatures separate into two regimes at about $\tau_c \approx 10$ years, with negative and positive logarithmic slopes = $\xi(2)/2 \approx -0.1, 0.4$ for $\Delta t < \tau_c$, and $\Delta t > \tau_c$, respectively. Since $\beta = 1 + \xi(2)$ (equation (11)), we have $\beta \approx 0.8, 1.8$. We also analyzed the
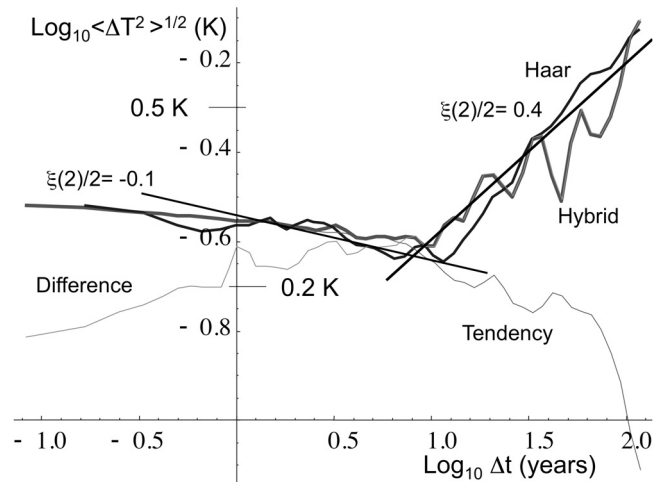
Figure 5. A comparison of the different structure function analyses (root-mean-square (RMS)) applied to the ensemble of three monthly surface series discussed in section 3.4 (NASA GISS, NOAA NCDC, and HadCRUT3), each globally averaged, from 1881 to 2008 (1548 points each). The usual (difference, poor man's) (bottom left) structure function (thin gray), (bottom right) the tendency structure function (thin gray), the maximum of the two ("Hybrid," thick, gray), and the Haar (in black) are shown. The latter has been increased by a factor $C = 10^{0.35} = 2.2$; the resulting RMS deviation with respect to the hybrid is $\pm 14\%$. Reference slopes with exponents $\xi(2)/2 \approx 0.4$ and -0.1 are also shown (corresponding to spectral exponents $\beta = 1 + \xi(2) = 1.8$ and 0.8, respectively). In terms of difference fluctuations, we can use the global RMS $\langle \Delta T(\Delta t)^2 \rangle^{1/2}$ annual structure functions (fitted for 129 years $> \Delta t > 10$ years), obtaining $\langle \Delta T(\Delta t)^2 \rangle^{1/2} \approx 0.08 \Delta t^{0.33}$ for the ensemble. In comparison, *Lovejoy and Schertzer* [1986] found the very similar $\langle \Delta T(\Delta t)^2 \rangle^{1/2} \approx 0.077 \Delta t^{0.4}$ using Northern Hemisphere data (these correspond to $\beta_c = 1.66$ and 1.8, respectively).

first-order structure function whose exponent $\xi(1) = H$; at these scales, the intermittency ($K(2)$, equation (4)) ≈ 0.03 so that $\xi(2) \approx 2H$ so that $H \approx -0.1, 0.4$ confirming that fluctuations decrease with scale in the low-frequency weather regime but increase again at lower frequencies in the climate regime (more precise intermittency analyses are given in the work of *Lovejoy and Schertzer* [2012]). Note that ignoring intermittency, the critical value of β discriminating between growing and decreasing fluctuations (i.e., $H < 0$, $H > 0$) is $\beta = 1$.

Before pursuing the Haar structure function, let us briefly consider its sensitivity to nonscaling perturbations, i.e., to nonscaling external trends superposed on the data, which break the overall scaling. Even when there is no particular reason to suspect such trends, the desire to filter them out is commonly invoked to justify the use of special wavelets, or nearly equivalently, of various orders of the multifractal detrended fluctuation analysis technique (MFDFA) [*Kantelhardt*

et al., 2002]. A simple way to produce a higher-order Haar wavelet that eliminates polynomials of order *n* is simply to iterate (*n* + 1 times) the difference operator in equation (14). For example, iterating it three times yields the "quadratic Haar" fluctuation $(\Delta v(\Delta t))_{\text{Haarquad}} = \frac{3}{\Delta t}(s(t + \Delta t) - 3s(t + \Delta t/3) + 3s(t - \Delta t/3) - s(t - \Delta t))$. This fluctuation is sensitive to structures of size Δt^{-1} and, hence, useful over the range $-1 < H < 2$, and it is blind to polynomials of order 1 (lines). In comparison, the *n*th-order DFA technique defines fluctuations using the RMS deviations of the summed series $s(t)$ from regressions of *n*th-order polynomials so that quadratic Haar fluctuations are nearly equivalent to the quadratic MFDFA RMS deviations (although these deviations are not strictly wavelets, note that the MFDFA uses a scaling function $\approx \Delta v \, \Delta t$; hence, with DFA exponent, $\alpha_{\text{DFA}} = 1 + H$). Although at first sight the insensitivity of these higher-order wavelets to trends may seem advantageous, it should be recalled that, on the one hand, they only filter out polynomial trends (and not, for example, the more geophysically relevant periodic trends), while on the other hand, even for this, they are "overkill" since the trends they filter are filtered at all scales, not just the largest. Indeed, if one suspects the presence of external polynomial trends, it suffices to eliminate them over the whole series (i.e., at the largest scales) and then to analyze the resulting deviations using the Haar fluctuations.

Figure 6 shows the usual (linear) Haar RMS structure function (equation (14)) compared to the quadratic Haar and quadratic MFDFA structure functions. Unsurprisingly, the latter two are close to each other (after applying different calibration constants, see the figure caption), that the low and
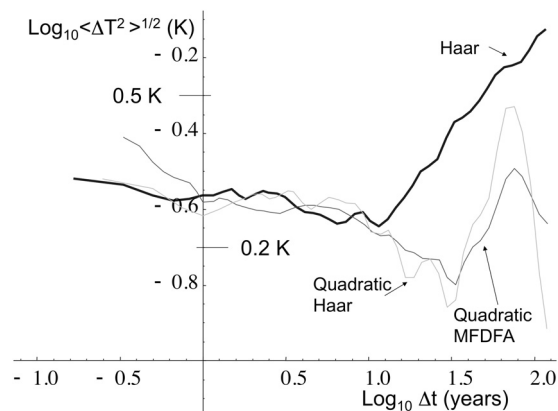
Figure 6. Same temperature data as Figure 5: a comparison of the RMS Haar structure function (multiplied by $10^{0.35} = 2.2$), the RMS quadratic Haar (multiplied by $10^{0.15} = 1.4$), and the RMS quadratic multifractal detrended fluctuation analysis (multiplied by $10^{1.5} = 31.6$).

high-frequency exponents are roughly the same. However, the transition point has shifted by nearly a factor of 3 so that, overall, they are rather different from the Haar structure function, and it is clearly not possible to simultaneously "calibrate" the high- and low-frequency parts. The drawback with these higher-order fluctuations is thus that we lose the simplicity of interpretation of the Haar wavelet, and unless $H > 1$, we obtain no obvious advantage.

4. THE TRANSITION FROM LOW-FREQUENCY WEATHER TO THE CLIMATE

### 4.1. Intermediate-Scale Multiproxy Series

In section 2, we discussed atmospheric variability over the frustratingly short instrumentally accessible range of time scales (roughly $\Delta t < 150$ years) and saw evidence that weakly variable low-frequency weather gives way to a new highly variable climate regime at a scale τ_c, somewhere in the range 10–30 years. In Figure 1a, we already glimpsed the much longer 1–100 kyr scales accessible primarily via ice core paleotemperatures (see also below); these confirmed that, at least when averaged over the last 100 kyr or so, the climate does indeed have a new scaling regime with fluctuations increasing rather than decreasing in amplitude with scale ($H > 0$).

Since the temporal resolution of the high-resolution Greenland Ice Core Project (GRIP) paleotemperatures was ≈ 5.2 years (and for the Vostok series ≈ 100 years), these paleotemperature resolutions do not greatly overlap the instrumental range; it is thus useful to consider other intermediates: the "multiproxy" series that have been developed following the work of *Mann et al.* [1998]. Another reason to use intermediate-scale data is because we are living in a climate epoch, which is exceptional in both its long- and short-term aspects. For example, consider the long stretch of relatively mild and stable conditions since the retreat of the last ice sheets about 11.5 kyr ago, the "Holocene." This epoch is claimed to be at least somewhat exceptional: it has even been suggested that such stability is a precondition for the invention of farming and thus for civilization itself [*Petit et al.*, 1999]. It is therefore possible that the paleoclimate statistics averaged over series 100 kyr or longer may not be as pertinent as we would like for understanding the current epoch. Similarly, at the high-frequency end of the spectrum, there is the issue of "twentieth century exceptionalism," a consequence of twentieth century warming and the probability that at least some of it is of anthropogenic, not natural origin. Since these affect a large part of the instrumental record, it is problematic to use the latter as the basis for extrapolations to centennial and millennial scales. In the following, we try to assess both

"exceptionalisms" in an attempt to understand the natural variability in the last few centuries.

4.2. The Holocene Exception: Climate Variability in Time and in Space

The high-resolution GRIP core gives a striking example of the difference between the Holocene and previous epochs in central Greenland (Figure 7). Even a cursory visual inspection of the figure confirms the relative absence of low-frequency variability in the current 10 kyr section compared to previous 10 kyr sections. To quantify this, we can turn to Figure 8, which compares the RMS Haar structure functions for both GRIP (Arctic) and Vostok (Antarctic) cores for both the Holocene 10 kyr section and for the mean and spread of the eight earlier 10 kyr sections. The GRIP Holocene curve is clearly exceptional, with the fluctuations decreasing with scale out to $\tau_c \approx 2$ kyr in scale and with $\xi(2)/2 \approx -0.3$. This implies a spectral exponent near the low-frequency weather value $\beta \approx 0.4$, although it seems that as before $\xi(2)/2 \approx 0.4$ ($\beta \approx 1.8$) for larger Δt. The main difference however is that τ_c is much larger than for the other series (see Table 1 for quantitative comparisons). The exceptionalism is quantified by noting that the corresponding RMS fluctuation function ($S(\Delta t)$) is several standard deviations below the average of the previous eight 10 kyr sections. In comparison (to the right in Figure 8), the Holocene period of the Vostok core is also somewhat exceptional, although less so: up to $\tau_c \approx 1$ kyr, it has $\xi(2)/2 \approx -0.3$ ($\beta \approx 0.4$), and it is more or less within one standard deviation limits of its mean, although τ_c is still large. Beyond scales of ≈ 1 kyr, its fluctuations start to increase;
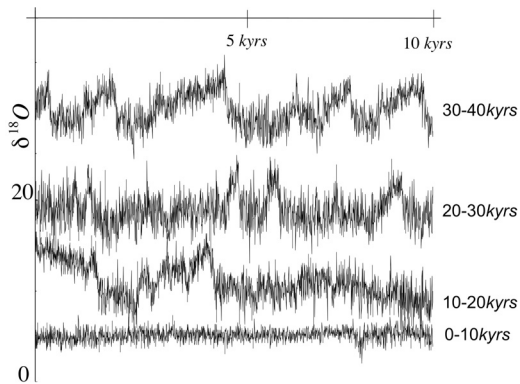
Figure 7. (bottom to top) Four successive 10 kyr sections of the high-resolution GRIP data, the most recent to the oldest. Each series is separated by 10 mils in the vertical for clarity (vertical units, mils, i.e., parts per thousand). The bottom Holocene series is indeed relatively devoid of low-frequency variability compared to the other 10 kyr sections, a fact confirmed by statistical analysis discussed in the text and Figure 8.
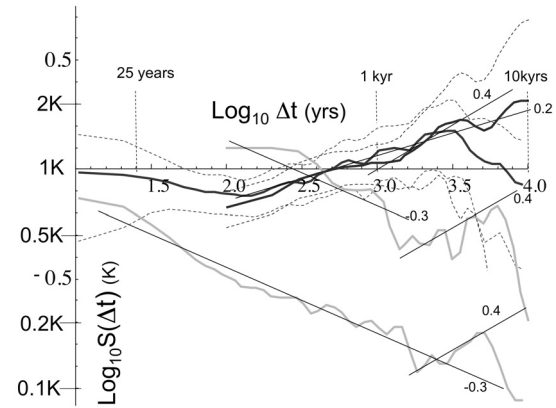
Figure 8. Comparison of the RMS Haar structure function ($S(\Delta t)$) for both Vostok and GRIP high-resolution cores (resolutions 5.2 and 50 years, respectively, over the last 90 kyr). The Haar fluctuations were calibrated and are accurate to ±20%. For Vostok, we used the *Petit et al.* [1999] calibration; for GRIP, we used 0.5 K mil^{-1}. The series were broken into 10 kyr sections. The thick gray lines show the most recent of these (roughly the Holocene, (top) Vostok, and (bottom) GRIP), whereas the long dark gray and short dark gray lines are the mean of the eight 10–90 kyr GRIP and Vostok $S(\Delta t)$ cores, respectively. The 1 standard deviation variations about the mean are indicated by dashed lines. Also shown are reference lines with slopes $\xi(2)/2 = -0.3$, 0.2, and 0.4 corresponding to $\beta = 0.4$, 1.4, and 1.8, respectively. Although the Holocene is exceptional for both series, for GRIP, it is exceptional by many standard deviations. For the Holocene, we can see that $\tau_c \approx 1$ kyr for Vostok and ≈ 2 kyr for GRIP, although for the previous 80 kyr, we see that $\tau_c \approx 100$ years for both.

Table 1 quantifies the differences. We corroborated this conclusion by an analysis of the 2 kyr long (yearly resolution) series from other (nearby) Greenland cores (as described by *Vinther et al.* [2008]) where *Blender et al.* [2006] also obtained $\beta \approx 0.2$–0.4 and also obtained similar low β estimates for the Greenland GRIP, GISP2 cores over the last 3 kyr.

Although these analyses convincingly demonstrate that the Greenland Holocene was exceptionally stable, nevertheless, their significance for the overall natural variations of Northern Hemisphere temperatures is doubtful. For example, on the basis of paleo-SST reconstructions just 1500 km southeast of Greenland [*Andersen et al.*, 2004; *Berner et al.*, 2008], it was concluded that the latter region was on the contrary "highly unstable." Using several ocean cores as proxies, Holocene SST reconstructions were produced, which included a difference between maximum and minimum of roughly 6 K and "typical variations" of 1–3 K. In comparison, from Figure 8, we see that the mean temperature fluctuation deduced from the GRIP core in the last 10 kyr is ≈ 0.2 K. However, also from Figure 8, we see that the mean

Table 1. Comparison of Various Paleoexponents Estimated Using the Haar Structure Function Over Successive 10 kyr Periods[a]

	H				β			
	Holocene		10–90 kyr		Holocene		10–90 kyr	
Range of regressions	100 years $< \Delta t$ < 2 kyr	2 kyr $< \Delta t$ < 10 kyr	100 years $< \Delta t$ < 10 kyr	100 years $< \Delta t$ < 10 kyr ensemble	100 years $< \Delta t$ < 2 kyr	2 kyr $< \Delta t$ < 10 kyr	100 years $< \Delta t$ < 10 kyr	100 years $< \Delta t$ < 10 kyr ensemble
GRIP	−0.25	0.21	0.14 ± 0.18	0.17	0.43	1.33	1.14 ± 0.33	1.20
Vostok	−0.40	0.38	0.19 ± 0.28	0.31	0.18	1.76	1.29 ± 0.51	1.49

[a]Vostok at 50 year resolution, Greenland Ice Core Project (GRIP) at 5.2 year resolution, all regressions over the scale ranges indicated. The Holocene is the most recent period (0–10 kyr). Note that while the Holocene exponents are estimates from individual series, the 10–90 kyr exponents are the means of the estimates from each 10 kyr section and (to the right) the exponent of the ensemble mean of the latter. Note that the mean of the exponents is a bit below the exponent of the mean indicating that a few highly variable 10 kyr sections can strongly affect the ensemble averages. For the Holocene, the separate ranges <2 kyr and $\Delta t > 2$ kyr were chosen because according to Figure 8, $\tau_c \approx 1$–2 kyr.

over the previous eight 10 kyr sections was ≈ 1–2 K, i.e., quite close to these paleo-SST variations (and about amount expected in order to explain the glacial/interglacial temperature swings, see section 5). These paleo-SST series thus underline the strong geographical climate variability effectively undermining the larger significance of the Greenland Holocene experience. At the same time, they lend support to the application of standard statistical stationarity assumptions to the variability over longer periods (e.g., to the relevance of spectra and structure functions averaged over the whole cores). Finally, *Lovejoy and Schertzer* [2012] argue that the spatial variability over both the low-frequency weather and climate regimes has very high intermittency and that this corresponds to the existence of climate zones.

4.3. Multiproxy Temperature Data, Centennial-Scale Variability, and the Twentieth Century Exception

The key to linking the long but geographically limited ice core series with the short but global-scale instrumental series are the intermediate category of "multiproxy temperature reconstructions." These series of Northern Hemisphere average temperatures, pioneered by *Mann et al.* [1998, 1999], have the potential of capturing "multicentennial" variability over at least the (data rich) Northern Hemisphere. These series are at typically annual resolutions and combine a variety of different data types ranging from tree rings, ice cores, lake varves, boreholes, ice melt stratigraphy, pollen, Mg/Ca variation in shells, ^{18}O in foraminifera, diatoms, stalactites (in caves), biota, and historical records. In what follows, we analyze eight of the longest of these (see Table 2 for some of statistical characteristics and descriptions).

Before reviewing the results, let us discuss some of the technical issues behind the continued development of new series. Consideration of the original series [*Mann et al.*,

1998] (extended back to 1000 A.D. by *Mann et al.* [1999]) illustrates both the technique and its attendant problems. The basic difficulty is in getting long series that are both temporally uniform and spatially representative. For example, the original six century long multiproxy series presented in the work of *Mann et al.* [1998] has 112 indicators going back to 1820, 74 to 1700, 57 to 1600, and only 22 to 1400. Since only a small number of the series go back more than two or three centuries, the series' "multicentennial" variability depends critically on how one takes into account the loss of data at longer and longer time intervals. When it first appeared, the Mann et al. series created a sensation by depicting a "hockey stick"-shaped graph of temperature, with the fairly flat "handle" continuing from 1000 A.D. until a rapid twentieth century increase. This lead to the famous conclusion, echoed in the IPPC Third Assessment Report [*Intergovernmental Panel on Climate Change*, 2001], that the twentieth century was the warmest century of the millennium, that the 1990s was the warmest decade, and that 1998 was the warmest year. This multiproxy success encouraged the development of new series using larger quantities of more geographically representative proxies [*Jones et al.*, 1998], by the introduction new types of data [*Crowley and Lowery*, 2000], to the more intensive use of pure dendrochronology [*Briffa et al.*, 2001], or to improved methodologies [*Esper et al.*, 2002].

However, the interest generated by reconstructions also attracted criticism, in particular, *McIntyre and McKitrick* [2003] pointed out several flaws in the *Mann et al.* [1998] data collection and in the application of the principal component analysis technique, which had been borrowed from econometrics. After correction, the same proxies yielded series with significantly larger low-frequency variability and included the reappearance of the famous "medieval warming" period at around 1400 A.D., which had disappeared in

Table 2. A Comparison of Parameters Estimated From the Multiproxy Data From 1500 to 1979 (480 Years)[a]

	β (High Frequency $(4–10 \text{ years})^{-1}$)	β (Lower Frequency Than $(25 \text{ years})^{-1}$)	H_{high} (4–10 years)	H_{low} (>25 years)
Jones et al. [1998]	0.52	0.99	−0.27	0.063
Mann et al. [1998, 1999]	0.57	0.53	−0.22	−0.13
Crowley and Lowery [2000]	2.28	1.61	0.72	0.31
Briffa et al. [2001]	1.19	1.18	0.15	0.13
Esper et al. [2002]	0.88	1.36	0.01	0.22
Huang [2004]	0.94	2.08	0.02	0.61
Moberg et al. [2005]	1.15	1.56	0.09	0.32
Ljundqvist [2010]	_	1.84	_	0.53

[a]The Ljundqvist high-frequency numbers are not given since the series has decadal resolution. Note that the β for several of these series was estimated by *Rybski et al.* [2006], but no distinction was made between low-frequency weather and climate; the entire series was used to estimate single (hence generally lower) β.

the original. Later, an additional technical critique [*McIntyre and McKitrick*, 2005] underlined the sensitivity of the methodology to low-frequency red noise variability present in the calibration data (the latter modeled this with exponentially correlated processes probably underestimating that which would have been found using long-range correlated scaling processes). Other work in this period, notably by *von Storch et al.* [2004] using "pseudo proxies" (i.e., the simulation of the whole calibration process with the help of GCMs), similarly underlined the nontrivial issues involved in extrapolating proxy calibrations into the past.

Beyond the potential social and political implications of the debate, the scientific upshot was that increasing attention had to be paid to the preservation of the low frequencies. One way to do this is to use borehole data, which, when combined with the use of the equation of heat diffusion, has essentially no calibration issues whatsoever. *Huang* [2004] used 696 boreholes (only back to 1500 A.D., roughly the limit of this approach) to augment the original [*Mann et al.*, 1998] proxies so as to obtain more realistic low-frequency variability. Similarly, in order to give proper weight to proxies with decadal and lower resolutions (especially lake and ocean sediments), *Moberg et al.* [2005] used wavelets to separately calibrate the low- and high-frequency proxies. Once again, the result was a series with increased low-frequency variability. Finally, *Ljundqvist* [2010] used a more up to date, more diverse collection of proxies to produce a decadal-resolution series going back to 1 A.D. The low-frequency variability of the new series was sufficiently large that it even included a third century "Roman warm period" as the warmest century on record and permitted the conclusion that "the controversial question whether Medieval Warm Period peak temperatures exceeded present temperatures remains unanswered" [*Ljundqvist*, 2010].

With this context, let us quantitatively analyze the eight series cited above; we use the Haar structure function. We concentrate here on the period 1500–1979 because (1) it is common to all eight reconstructions, (2) being relatively recent, it is more reliable (it has lower uncertainties), and (3) it avoids the Medieval Warm Period and thus the possibility that the low-frequency variability is artificially augmented by the possibly unusual warming in the 1300s. The result is shown in Figure 9, where we have averaged the structure functions into the five pre-2003 and three post-2003 reconstructions. Up to $\Delta t \approx 200$ years, the basic shapes of the curves are quite similar to each other and, indeed, to the surface temperature $S(\Delta t)$ curves back to 1881 (Figure 5). However, quite noticeable for the pre-2003 constructions is the systematic drop in RMS fluctuations for $\Delta t \approx >200$ years, which contrasts with their continued rise in the post-2003 reconstructions. This confirms the above analysis to the effect that the post-2003 analyses were more careful in their treatments of multicentennial variability. Table 2 gives a quantitative intercomparison of the various statistical parameters.

Figure 9 compares the mean multiproxies with the ensemble average of the instrumental global surface series. This confirms the basic behavior: small Δt scaling with $\xi(2)/2 = -0.1$ (β = 0.8) followed by large Δt scaling with $\xi(2)/2 = 0.4$ (β = 1.8) is displayed by all the data, all the pre-2003 $S(\Delta t)$ functions drop off for $\Delta t \approx >200$ years. Notable are (1) the transition scale in the global instrumental temperature at $\tau_c \approx 10$ years, which is somewhat lower than that found in the multiproxy reconstructions ($\tau_c \approx 40–100$ years) and (2) over the common low-frequency part that the amplitudes of the reconstruction RMS fluctuations are about a factor of 2 lower than for the global instrumental series. The reason for the amplitude difference is not at all clear since, on the one hand, the monthly and annually averaged Haar structure functions of the instrumental series are very close to each other up to $\Delta t \approx 10$ years (the temporal resolution is not an issue), and similarly, the difference between the Northern Hemisphere
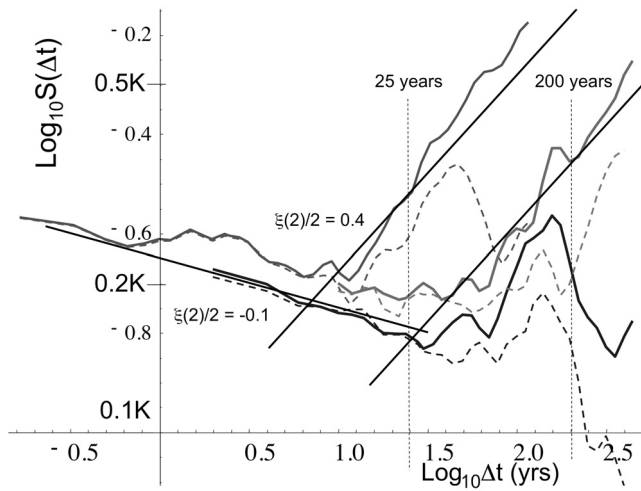
Figure 9. (bottom) RMS Haar fluctuation for the mean of the pre-2003 and post-2003 series from 1500 to 1979 (solid black and gray curves, respectively, and excluding the Crowley series due to its poor resolution), along with (top) the mean of the globally averaged monthly resolution surface series from Figure 5 (solid gray). In order to assess the effect of the twentieth century warming, the structure functions for the multiproxy data were recalculated from 1500 to 1900 only (the associated thin dashed lines) and for the instrumental surface series with their linear trends from 1880 to 2008 removed (the data from 1880 to 1899 are too short to yield a meaningful $S(\Delta t)$ estimate for the lower frequencies of interest). While the large Δt variability is reduced a little, the basic power law trend is robust, especially for the post-2003 reconstructions. Note that the decrease in $S(\Delta t)$ for the linearly detrended surface series over the last factor of 2 or so in lag Δt is a pure artifact of the detrending. We may conclude that the low-frequency rise is not an artifact of an external linear trend. Reference lines corresponding to $\beta = 0.8$ and 1.8 have been added.

and the Southern Hemisphere instrumental $S(\Delta t)$ functions is much smaller than this (only about ≈15%).

To get another perspective on this low-frequency variability, we can compare the instrumental and multiproxy structure functions with those from ice core paleotemperature discussed in more detail in the next section. In Figure 10, we have superposed the calibrated deuterium-based RMS temperature fluctuations with RMS multiproxy and RMS surface series fluctuations (we return to this in section 5). We see that extrapolating the latter out to 30–50 kyr is quite compatible with the Vostok core with the "interglacial window" (i.e., the rough quasiperiod and amplitude corresponding to the interglacials). Although the Vostok $S(\Delta t)$ curve is from the entire 420 kyr record (not just the Holocene), this certainly makes it plausible that while the surface series appear to have realistic low-frequency variability, the variability of the reconstructions is too small (although the post-2003 reconstructions are

indeed more realistic than the contrasting relative lack of variability in the pre-2003 reconstructions).

4.4. Twentieth Century Exceptionalism

Although the reconstructions and instrumental series qualitatively agree, their quantitative disagreement is large and requires explanation. In this section, we consider whether this could be a consequence of the twentieth century "exceptionalism" discussed earlier, the fact that, irrespective of the cause, the twentieth century is somewhat warmer than the nineteenth and earlier centuries. It has been recognized that this warming causes problems for the calibration of the proxies [e.g., *Ljundqvist*, 2010], and it will clearly contribute to the RMS multicennial variability in Figure 9. In order to demonstrate that the basic type of statistical variability is not an artifact of the inclusion of exceptional twentieth century temperatures in Figure 9, we also show the corresponding Haar structure functions for the earlier period 1500–1900. Truncating the instrumental series at 1900 would result in a series only 20 years long; therefore, the closest equivalent for the surface series was to remove overall linear trends and then redo the analysis. As expected, the figure shows that all the large Δt fluctuations are reduced but that the basic scaling behaviors are apparently not affected. We conclude that both the type of variability as characterized by the scaling exponents and the transition scale τ_c are fairly robust, if difficult,
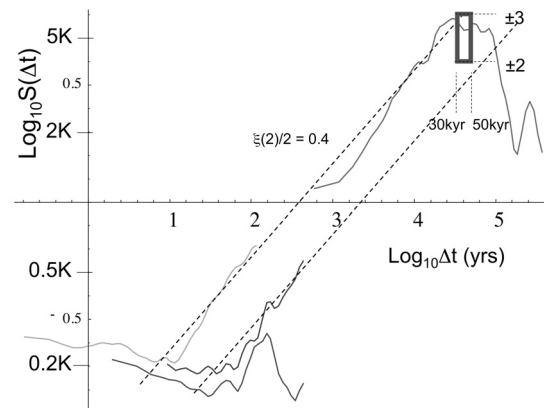
Figure 10. (bottom left) RMS Haar fluctuations for the mean monthly, global surface series (thin gray, from Figure 5) and (bottom right) the mean pre-2003 (medium gray) and (bottom middle) mean post-2003 proxies (dark gray, from Figure 9) as well as the mean (top right) Vostok $S(\Delta t)$ function over the last 420 kyr interpolated to 300 year resolution and using the *Petit et al.* [1999] calibration. Also shown (the rectangle) is the "interglacial window," the probable typical range of fluctuations and quasiperiods of the glacial-interglacials. The "calibration" of the fluctuation amplitudes is accurate to ±25%.

to accurately determine; they are not artifacts of external linear trends. The instrumental and reconstruction discrepancy in Figure 9 thus remains unexplained.

5. TEMPORAL SPECTRAL SCALING IN THE CLIMATE REGIME: 10–10⁵ YEARS

5.1. Review of Literature

Thanks to several ambitious international projects, many ice cores exist, particularly from the Greenland and Antarctic ice sheets, which provide surrogate temperatures based on $\delta^{18}O$ or deuterium concentrations in the ice. The most famous cores are probably the GRIP and Vostok (Antarctica) cores, each of which are over 3 km long (limited by the underlying bedrock) and go back, respectively, 240 and 420 kyr. Near the top of the cores, individual annual cycles can be discerned (in some cases, going back over 10 kyr); below that, the shearing of ice layers and diffusion between the increasingly thin annual layers make such direct dating impossible, and models of the ice flow and compression are required. Various "markers" (such as dust layers from volcanic eruptions) are also used to help fix the core chronologies.

A problem with the surrogates is their highly variable temporal resolutions combined with strong depth dependences. For example, *Witt and Schumann* [2005] used wavelets, *Davidsen and Griffin* [2010] used (monofractal) fractional Brownian motion as a model, and *Karimova et al.* [2007] used (mono) fractal interpolation to attempt to handle this; *Lovejoy and Schertzer* [2012] found that the temporal resolution itself has multifractal intermittency. The main consequence is that the intermittency of the interpolated surrogates is a bit too high but that serious spectral biases are only present at scales of the order of the mean resolution or higher frequencies.

With these caveats, Table 3 summarizes some of the spectral scaling exponents, scaling ranges. It is interesting to note that the three main orbital ("Milankovitch") forcings at 19, 23 (precessional), and 41 kyr (obliquity) are indeed visible, but only barely, above the scaling "background" [see especially *Wunsch*, 2003].

5.2. A Composite Picture of Atmospheric Variability From 6 Hours to 10⁵ Years

To clarify our ideas about the variability, it is useful to combine data over huge ranges of scale into a single composite analysis (such as the spectra shown in Figures 1a, 1b) but using real space fluctuations rather than spectra. Some time ago, such a composite already clarified the following points: (1) that there is a distinction between the variability of regional- and global-scale temperatures, (2) that global averages had particularly small transition scale τ_c, (3) that there was a scaling range for global averages between scales of about 3 years and 40–50 kyr (where the variability apparently "saturates") with a realistic exponent $\beta_c \approx 1.8$, and (4)

Table 3. An Intercomparison of Various Estimates of the Spectral Exponents β_c of the Low-Frequency Climate Regime and Scaling Range Limits[a]

| Series	Authors	Series Length (kyr)	Resolution (years)	β_c
Composite ice cores, instrumental	*Lovejoy and Schertzer* [1986]	10^{-9} to 1000	1000	1.8
Composite (Vostok) (ice core, instrumental)	*Pelletier* [1998]	10^{-5} to 1000	0.1 to 500	2
$\delta^{18}O$ from GRIP Greenland	*Wunsch* [2003]	100	100	1.8
Planktonic $\delta^{18}O$ ODP677 (Panama basin)	*Wunsch* [2003]	1000	300	2.3
CO_2, Vostok (Antarctica)	*Wunsch* [2003]	420	300	1.5
$\delta^{18}O$ from GRIP Greenland	*Ditlevsen et al.* [1996]	91	5	1.6
$\delta^{18}O$ from GRIP Greenland	*Schmitt et al.* [1995]	123	200	1.4
$\delta^{18}O$ from GISP Greenland	*Ashkenazy et al.* [2003]	110	100	1.3
$\delta^{18}O$ from GRIP Greenland	*Ashkenazy et al.* [2003]	225	100	1.4
$\delta^{18}O$ from Taylor (Antarctica)	*Ashkenazy et al.* [2003]	103	100	1.8
$\delta^{18}O$ from Vostok	*Ashkenazy et al.* [2003]	420	100	2.1
Composite, midlatitude	*Huybers and Curry* [2006]	10^{-4} to 1000	0.1 to 10^3	1.6
Composite tropics	*Huybers and Curry* [2006]	10^{-4} to 1000	0.1 to 10^3	1.3
$\delta^{18}O$ from GRIP Greenland	*Lovejoy and Schertzer* [2012]	91	5	1.4
$\delta^{18}O$ from Vostok	*Lovejoy and Schertzer* [2012]	420	300	1.7
$\delta^{18}O$ from GRIP, Greenland	*Blender et al.* [2006]	3	3	0.4
$\delta^{18}O$ from GISP2 Greenland	*Blender et al.* [2006]	3	3	0.7
$\delta^{18}O$ from GRIP Greenland (last 10 kyr only)	Figure 8	10	5	0.2

[a]For series with resolution ≈100 years, the last three rows are for the (anomalous) Holocene only [see *Lovejoy and Schertzer*, 2012].

that this scaling regime could potentially quantitatively explain the magnitudes of the temperature swings between interglacials [*Lovejoy and Schertzer*, 1986].

Similar scaling composites, but in Fourier space, were adopted by *Pelletier* [1998] and, more recently, by *Huybers and Curry* [2006], who made a more data-intensive study of the scaling of many different types of paleotemperatures collectively spanning the range of about 1 month to nearly 10^6 years. The results are qualitatively very similar, including the positions of the scale breaks; the main innovations are (1) the increased precision on the β estimates and (2) the basic distinction made between continental and oceanic spectra including their exponents. We could also mention the composite of *Fraedrich et al.* [2009], which is a modest adaptation of that of *Mitchell* [1976], although it does introduce a single scaling regime spanning only 2 orders of magnitude: from ≈3 to ≈100 years (with β ≈ 0.3), at lower frequencies, the composite exhibits a *decrease* (rather than *increase*) in variability.

Figure 11 shows an updated composite where we have combined the 20CR reanalysis spectra (both local, single grid point and global) with the GRIP 55 cm and GRIP high-resolution spectra (both for the last 10 kyr and averaged over the last 90 kyr), and the three surface global temperature series. For reference, we have also included the 500 year control run of the Institut Pierre Simon Laplace (IPSL) GCM used in the IPCC Fourth Assessment Report. We use difference structure functions so that the interpretation is particularly simple, although a consequence (see section 3.3) is that all the logarithmic slopes are >0. In order to avoid this problem, compare this to the Haar structure functions (Figure 12).

Key points to note are (1) the use of annually averaged instrumental data in Figure 11 (differences), but of daily data in Figure 12 (Haar) and (2) the distinction made between globally and locally averaged quantities whose low-frequency weather have different scaling exponents. Also shown is the interglacial window (Δt is the half quasiperiod, and for a white noise, S is double the amplitude). The calibration of the paleotemperatures is thus constrained so that it goes through the window at large Δt but joins up to the *local* instrumental S(Δt) at small Δt. In addition, as discussed in Section 4.2, since the last 10 kyr GRIP fluctuations are anomalously low (Figure 4 and see the nearly flat red curve compared with the full 91 kyr red curve), the calibration must be based on this flatter S(Δt) (Figure 11). Starting at τ_c ≈ 10 years, one can plausibly extrapolate the global S(Δt) using H = 0.4 (β ≈ 1.8), all the way to the interglacial window (with nearly an identical S(Δt) as given by *Lovejoy and Schertzer* [1986]), although the Northern Hemisphere reconstructions do not extrapolate as well, possibly because of their higher intermittency. The local temperatures extrapolate (starting at τ_c ≈
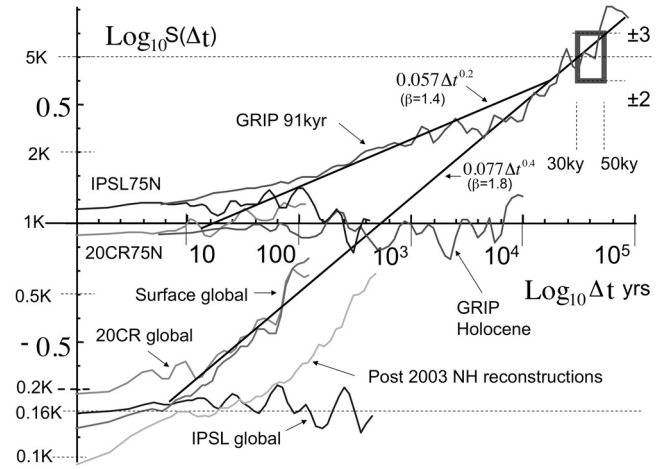
Figure 11. (top right) A comparison of the RMS structure function S(Δt) of the high-resolution (5.2 year) GRIP (gray), IPSL (top left) 75°N and (bottom left) global, 20CR (top) 75°N (light gray) and (bottom) global (light gray), (bottom left) mean surface series (darker gray), (bottom left) mean of the three post-2003 Northern Hemisphere reconstructions (light gray) for globally averaged temperatures, and (top) the mean at Greenland latitudes, all using fluctuations defined as differences (poor man's wavelet) so that the vertical scale directly indicates typical changes in temperature. In addition, the GRIP data are divided into two groups: the Holocene (taken as the last 10 kyr, along the axis) and (top right) the entire 91 kyr of the high-resolution GRIP series (gray). The GRIP $\delta^{18}O$ data have been calibrated by lining up the Holocene structure function with the mean 75°N 20CR reanalysis structure function (corresponding to ≈0.65 K mil^{-1}). When this is done, the 20CR and surface mean global structure functions can be extrapolated with exponent H ≈ 0.4 (see the corresponding line) to the "interglacial window" (box) corresponding to half pseudoperiods between 30 and 50 kyr with variations (= ±S/2) between ±2 and ±3 K. This line corresponds to spectral exponent β = 1.8. Finally, we show a line with slope ξ(2)/2 = 0.2, corresponding to the GRIP β = 1.4 (see Figures 1a and 1b); we can see that extrapolating it to 50 kyr explains the local temperature spectra quite well.

20 years) with a lower exponent corresponding to β ≈ 1.4 (see Figure 1a), which is close to the other Greenland paleotemperature exponents (Table 3) presumably reflecting the fact that the Antarctic temperatures are better surrogates for global rather than local temperatures; these exponents are all averages over spectra of series of ≈100 kyr or more in length. An interesting feature of the Haar structure function (Figure 12) is that it shows that local (grid scale) temperature fluctuations are roughly the same amplitude for monthly as for the much longer glacial/interglacials periods. Not only can we make out the three scaling regimes discussed above but also for Δt > 100 kyr, we can start to discern a new "low-

Figure 12. The equivalent of Figure 11 except for the RMS Haar structure function rather than the RMS difference structure function and including daily resolution 20CR data and monthly resolution surface temperatures. We show (top left) grid point scale ($2° \times 2°$) daily scale fluctuations for both 75°N and globally averaged along with reference slope $\xi(2)/2 \approx H = -0.4$ (20CR, 700 mb). We see (lower left) at daily resolution, the corresponding globally averaged structure function. Also shown are the average of the three in situ surface series (Figure 5) as well as the post-2003 multiproxy structure function (from Figure 9). We show (right) both the GRIP (55 cm resolution, calibrated with 0.5 K mil^{-1}) and the Vostok paleotemperature series. All the fluctuations have been multiplied by 2.2 so that the calibration scale in degrees K is fairly accurate (compare with Figure 11). Also shown are the interglacial window and a reference line with slope -0.5 corresponding to Gaussian white noise.

frequency climate" regime. For more scaling paleoclimate analyses, including "paleocascades," see the work of *Lovejoy and Schertzer* [2012].

6. CONCLUSIONS

Just as the laws of continuum mechanics emerge from those of statistical mechanics when large enough numbers of particles are present, so do the laws of turbulence emerge at high-enough Reynold's numbers and at strong-enough nonlinearity. However, the classical turbulence laws were constrained by strong assumptions of homogeneity and isotropy and could not cover wide scale ranges in the atmosphere. By generalizing them to take into account anisotropy (especially vertical stratification) and intermittency, their range of applicability is vastly increased. In the last 5 years, thanks in part to the ready availability of huge global-scale data sets of all kinds, it has been possible to verify that these generalized emergent laws accurately hold up to planetary

scales. For a recent review, see the work of *Lovejoy and Schertzer* [2010].

These "weather regime" laws show that the horizontal variability is fundamentally controlled by solar forcing via the energy flux. First principle calculations show that this accurately accounts for the large-scale winds and predicts a drastic "dimensional transition" at $\tau_w \approx 10$ days, the typical lifetime of planetary-scale structures. Beyond this time scale, spatial interactions are rapidly quenched so that the longer scales are driven by essentially temporal degrees of freedom, and the spectra of atmospheric fields display a shallow "spectral plateau" with small logarithmic slope. By making a third generalization of the classical laws, the statistical behavior in this "low-frequency weather" regime can be predicted. This qualitative change in the statistics at τ_w is just as expected; it is neither due to the action of new mechanisms of internal variability nor to external climate forcing; it is apparently nothing more than low-frequency weather. Similarly (forcing free), GCM control runs reproduce the same type of variability out to their low-frequency limits. The main complication is that due to similar effects from ocean turbulence, whose corresponding outer time scale is $\tau_o \approx 1$ year, there is enhanced intermittency up to that scale, with a slightly steeper "low-frequency ocean weather" regime beyond. Depending on the location and atmospheric variable of interest, this scaling continues up to scales of ≈10–100 years beyond which the type of variability drastically changes; new mechanisms of internal variability or of external climate forcing must come into play: the true climate regime begins. It is notable that if we consider pre-twentieth century Northern Hemisphere temperatures, the result is qualitatively similar so that, presumably, anthropogenic forcings are not responsible for this new regime.

In section 2, we discussed the weather and low-frequency weather regimes using spectral techniques. However, in later sections, we turned to real space fluctuation statistics. For these, the key parameter is the fluctuation exponent H, which determines the rate at which the mean fluctuations increase ($H > 0$) or decrease ($H < 0$) with scale Δt. We underlined the particularly simple interpretations afforded by the usual difference and tendency structure functions. However, the corresponding wavelets only usefully characterize the scaling of the fluctuations over narrow ranges in the exponent H: the differences ($0 < H < 1$) and the tendency ($-1 < H < 0$), i.e., useful only for fluctuations increasing in amplitude with scale or decreasing in amplitude with scale, respectively. Since both the weather and climate generally have $H > 0$ and the low-frequency weather regime has $H < 0$, we instead defined fluctuations using the Haar wavelet, which is thus useful over the entire range $-1 < H < 1$ and can also be

"calibrated" to directly yield fluctuation amplitudes and can be easily implemented numerically.

In order to evaluate the statistical variability of the atmosphere over as wide a range as possible, we combined the Haar wavelet with temperature data from the 20CR (1871–2008), (2° × 2°, 6 hourly), three surface series (5° × 5°, monthly), eight intermediate-length resolution "multiproxy" series of the Northern Hemisphere from 1500 to 1980 (yearly), and GRIP and Vostok paleotemperatures at 5.2 and ≈100 year resolutions over lengths 91 and 420 kyr. The basic findings were that the key transition scale τ_c from low-frequency weather to climate, was somewhat variable, depending on the field and geographical location. For example, for surface global temperatures, we found $\tau_c \approx 10$ years, whereas for the more reliable post-2003 Northern Hemisphere reconstructions, $\tau_c \approx 30$ years, for the Holocene GRIP (Greenland) core, $\tau_c \approx 2$ kyr, the Holocene Vostok (Antarctica) core, $\tau_c \approx 1$ kyr, and the mean pre-Holocene paleotemperature value, $\tau_c \approx 100$ years. We also found $H_{lw} \approx -0.4$ and -0.1 for local (e.g., 2° × 2° resolution) and global series, respectively, and $H_c \approx 0.4$; although the GRIP value was a little lower, these values correspond to $\beta_{lw} \approx 0.2, 0.8, 1.8$, respectively (ignoring intermittency corrections $K(2)$, which ranged from $K_{lw}(2) \approx 0.05$ to $K_c(2) \approx 0.1$; a full characterization of the intermittency, i.e., $K(q)$ was been performed but was not discussed here).

Although this basic overall three-scaling regime picture is 25 years old, much has changed to make it more convincing. Obviously, an important element is the improvement in the quantity and quality of the data, but we have also benefited from advances in nonlinear dynamics as well as in data analysis techniques. In combination, these advances make the model a seductive framework for understanding atmospheric variability over huge ranges of space-time scales. It allows us to finally clarify the distinction between weather, its straightforward extension, without new elements, to low-frequency weather, and finally to the climate regime. It allows for objective definitions of the weather (scales $<\tau_w$), climate states (averages up to τ_c), and hence of climate change (scales $>\tau_c$). This new understanding of atmospheric variability is essential for evaluating the realism of both atmospheric and climate models. In particular, since without special external forcing, GCMs only model low-frequency weather, the question is posed as to what types of external forcing are required so that the GCM variability makes a transition to the climate regime with realistic scaling exponents and at a realistic time scales.

REFERENCES

Andersen, C., N. Ko, and M. Moros (2004), A highly unstable Holocene climate in the subpolar North Atlantic: Evidence from diatoms, *Quat. Sci. Rev.*, *23*, 2155–2166.

Ashkenazy, Y., D. R. Baker, H. Gildor, and S. Havlin (2003), Nonlinearity and multifractality of climate change in the past 420,000 years, *Geophys. Res. Lett.*, *30*(22), 2146, doi:10.1029/2003GL018099.

Ashok, V., T. Balakumaran, C. Gowrishankar, I. L. A. Vennila, and A. Nirmalkumar (2010), The fast Haar wavelet transform for signal and image processing, *Int. J. Comput. Sci. Inf. Security*, *7*, 126–130.

Bacry, A., A. Arneodo, U. Frisch, Y. Gagne, and E. Hopfinger (1989), Wavelet analysis of fully developed turbulence data and measurement of scaling exponents, in *Turbulence and Coherent Structures*, edited by M. Lessieur and O. Metais, pp. 703–718, Kluwer Acad., Dordrecht, Netherlands.

Berner, K. S., N. Koç, D. Divine, F. Godtliebsen, and M. Moros (2008), A decadal-scale Holocene sea surface temperature record from the subpolar North Atlantic constructed using diatoms and statistics and its relation to other climate parameters, *Paleoceanography*, *23*, PA2210, doi:10.1029/2006PA001339.

Blender, R., and K. Fraedrich (2003), Long time memory in global warming simulations, *Geophys. Res. Lett.*, *30*(14), 1769, doi:10.1029/2003GL017666.

Blender, R., K. Fraedrich, and B. Hunt (2006), Millennial climate variability: GCM-simulation and Greenland ice cores, *Geophys. Res. Lett.*, *33*, L04710, doi:10.1029/2005GL024919.

Bolgiano, R., Jr. (1959), Turbulent spectra in a stably stratified atmosphere, *J. Geophys. Res.*, *64*(12), 2226–2229.

Briffa, K., T. Osborn, F. Schweingruber, I. Harris, P. Jones, S. Shiyatov, and E. Vaganov (2001), Low-frequency temperature variations from a northern tree ring density network, *J. Geophys. Res.*, *106*(D3), 2929–2941.

Brunt, D. (1939), *Physical and Dynamical Meteorology*, 2nd ed., 454 pp., Cambridge Univ. Press, New York.

Bunde, A., J. F. Eichner, S. Havlin, E. Koscielny-Bunde, H. J. Schellnhuber, and D. Vyushin (2004), Comment on "Scaling of atmosphere and ocean temperature correlations in observations and climate models," *Phys. Rev. Lett.*, *92*, 039801, doi:10.1103/PhysRevLett.92.039801.

Burgert, R., and W. W. Hsieh (1989), Spectral analysis of the AVHRR sea surface temperature variability off the west coast of Vancouver Island, *Atmos. Ocean*, *27*, 577–587.

Clayson, C. A., and L. H. Kantha (1999), Turbulent kinetic energy and its dissipation rate in the equatorial mixed layer, *J. Phys. Oceanogr.*, *29*, 2146–2166.

Compo, G. P., et al. (2011), The Twentieth Century Reanalysis Project, *Q. J. R. Meteorol. Soc.*, *137*, 1–28.

Corrsin, S. (1951), On the spectrum of isotropic temperature fluctuations in an isotropic turbulence, *J. Appl. Phys.*, *22*, 469–473.

Crowley, T. J., and T. S. Lowery (2000), How warm was the Medieval Warm period?, *Ambio*, *29*, 51–54.

Davidsen, J., and J. Griffin (2010), Volatility of unevenly sampled fractional Brownian motion: An application to ice core records, *Phys. Rev. E*, *81*, 016107, doi:10.1103/PhysRevE.81.016107.

Deschamps, P. Y., R. Frouin, and L. Wald (1981), Satellite determination of the mesoscale variability of the sea surface temperature, *J. Phys. Oceanogr.*, *11*, 864–870.

Deschamps, P., R. Frouin, and M. Crépon (1984), Sea surface temperatures of the coastal zones of France observed by the HCMM satellite, *J. Geophys. Res.*, *89*(C5), 8123–8149.

Ditlevsen, P. D., H. Svensmark, and S. Johson (1996), Contrasting atmospheric and climate dynamics of the last-glacial and Holocene periods, *Nature*, *379*, 810–812.

Eichner, J. F., E. Koscielny-Bunde, A. Bunde, S. Havlin, and H.-J. Schellnhuber (2003), Power-law persistence and trends in the atmosphere: A detailed study of long temperature records, *Phys. Rev. E*, *68*, 046133, doi:10.1103/PhysRevE.68.046133.

Esper, J., E. R. Cook, and F. H. Schweingruber (2002), Low-frequency signals in long tree-ring chronologies for reconstructing past temperature variability, *Science*, *295*(5563), 2250–2253.

Fraedrich, K., and K. Blender (2003), Scaling of atmosphere and ocean temperature correlations in observations and climate models, *Phys. Rev. Lett.*, *90*, 108501, doi:10.1103/PhysRevLett.90.108501.

Fraedrich, K., R. Blender, and X. Zhu (2009), Continuum climate variability: Long-term memory, scaling, and 1/f-noise, *Int. J. Mod. Phys. B*, *23*, 5403–5416.

Goldman, J. L. (1968), The power spectrum in the atmosphere below macroscale, *TRECOM 365G5-F*, Inst. of Desert Res., Univ. of St. Thomas, Houston, Tex.

Grant, H. L., R. W. Steward, and A. Moillet (1962), Turbulence spectra from a tidal channel, *J. Fluid Mech.*, *2*, 263–272.

Hansen, J., R. Ruedy, M. Sato, and K. Lo (2010), Global surface temperature change, *Rev. Geophys.*, *48*, RG4004, doi:10.1029/2010RG000345.

Holschneider, M. (1995), *Wavelets: An Analysis Tool*, 423 pp., Clarendon, New York.

Huang, S. (2004), Merging information from different resources for new insights into climate change in the past and future, *Geophys. Res. Lett.*, *31*, L13205, doi:10.1029/2004GL019781.

Huybers, P., and W. Curry (2006), Links between annual, Milankovitch and continuum temperature variability, *Nature*, *441*, 329–332.

Hwang, H. J. (1970), Power density spectrum of surface wind speed on Palmyra island, *Mon. Weather Rev.*, *98*, 70–74.

Inoue, E. (1951), On the turbulent diffusion in the atmosphere, *J. Meteorol. Soc. Jpn.*, *29*, 32.

Intergovernmental Panel on Climate Change (2001), *Climate Change 2001: The Scientific Basis: Contribution of Working Group I to the Third Assessment Report of the Intergovernmental Panel on Climate Change*, edited by J. T. Houghton et al., 881 pp., Cambridge Univ. Press, New York.

Intergovernmental Panel on Climate Change (2007), *Climate Change 2007: The Physical Science Basis: Working Group I Contribution to the Fourth Assessment Report of the IPCC*, edited by S. Solomon et al., Cambridge Univ. Press, New York.

Jones, P. D., K. R. Briffa, T. P. Barnett, and S. F. B. Tett (1998), High-resolution paleoclimatic records for the last Millenium: Interpretation, integration and comparison with General Circulation Model control-run temperatures, *Holocene*, *8*, 477–483.

Kantelhardt, J. W., E. Koscielny-Bunde, H. H. A. Rego, S. Havlin, and S. Bunde (2001), Detecting long range correlations with detrended fluctuation analysis, *Physica A*, *295*, 441–454.

Kantelhardta, J. W., S. A. Zschiegner, E. Koscielny-Bunde, S. Havlin, A. Bundea, and H. E. Stanley (2002), Multifractal detrended fluctuation analysis of nonstationary time series, *Physica A*, *316*, 87–114.

Karimova, L., Y. Kuandykov, N. Makarenko, M. M. Novak, and S. Helama (2007), Fractal and topological dynamics for the analysis of paleoclimatic records, *Physica A*, *373*, 737–746.

Kolesnikov, V. N., and A. S. Monin (1965), Spectra of meteorological field fluctuations, *Izv. Acad. Sci. USSR Atmos. Oceanic Phys., Engl. Transl.*, *1*, 653–669.

Kolmogorov, A. N. (1941), Local structure of turbulence in an incompressible liquid for very large Reynolds numbers, *Dokl. Akad. Nauk. SSSR*, *30*, 301–305. [English translation: *Proc. R. Soc. London, Ser. A*, *434*, 9–17, 1991]

Koscielny-Bunde, E., A. Bunde, S. Havlin, H. E. Roman, Y. Goldreich, and H.-J. Schellnhuber (1998), Indication of a universal persistence law governing atmospheric variability, *Phys. Rev. Lett.*, *81*, 729–732.

Koscielny-Bunde, E., J. W. Kantelhardt, P. Braund, A. Bunde, and S. Havlin (2006), Long-term persistence and multifractality of river runoff records: Detrended fluctuation studies, *J. Hydrol.*, *322*, 120–137.

Landau, L. D., and E. M. Lifschitz (1959), *Fluid Mechanics*, 536 pp., Pergamon, London, U. K.

Lanfredi, M., T. Simoniello, V. Cuomo, and M. Macchiato (2009), Discriminating low frequency components from long range persistent fluctuations in daily atmospheric temperature variability, *Atmos. Chem. Phys.*, *9*, 4537–4544.

Lennartz, S., and A. Bunde (2009), Trend evaluation in records with long-term memory: Application to global warming, *Geophys. Res. Lett.*, *36*, L16706, doi:10.1029/2009GL039516.

Le Traon, P. Y., P. Klein, B. L. Hua, and G. Dibarboure (2008), Do altimeter wavenumber spectra agree with the interior or surface quasigeostrophic theory?, *J. Phys. Oceanogr.*, *38*, 1137–1142.

Lien, R.-C., and E. A. D'Asaro (2006), Measurement of turbulent kinetic energy dissipation rate with a Lagrangian float, *J. Atmos. Oceanic Technol.*, *23*, 964–976.

Ljundqvist, F. C. (2010), A new reconstruction of temperature variability in the extra-tropical Northern Hemisphere during the last two millennia, *Geogr. Ann. Ser. A*, *92*, 339–351.

Lorenz, E. N. (1995), *Climate is What You Expect*, 55 pp., MIT Press, Cambridge, Mass.

Lovejoy, S., and D. Schertzer (1986), Scale invariance in climatological temperatures and the spectral plateau, *Ann. Geophys., Ser. B*, *4*, 401–410.

Lovejoy, S., and D. Schertzer (2010), Towards a new synthesis for atmospheric dynamics: Space-time cascades, *Atmos. Res.*, *96*, 1–52, doi:10.1016/j.atmosres.2010.01.004.

Lovejoy, S., and D. Schertzer (2012), *The Weather and Climate: Emergent Laws and Multifractal Cascades*, 660 pp., Cambridge Univ. Press, Cambridge, U. K.

Lovejoy, S., Y. Tessier, M. Claeredeboudt, W. J. C. Currie, J. Roff, E. Bourget, and D. Schertzer (2000), Universal multifractals and ocean patchiness phytoplankton, physical fields and coastal heterogeneity, *J. Plankton Res.*, *23*, 117–141.

Lovejoy, S., D. Schertzer, M. Lilley, K. B. Strawbridge, and A. Radkevitch (2008), Scaling turbulent atmospheric stratification. I: Turbulence and waves, *Q. J. R. Meteorol. Soc.*, *134*, 277–300, doi:10.1002/qj.201.

Mallat, S., and W. Hwang (1992), Singularity detection and processing with wavelets, *IEEE Trans. Inf. Theory*, *38*, 617–643.

Mann, M. E., R. S. Bradley, and M. K. Hughes (1998), Global-scale temperature patterns and climate forcing over the past six centuries, *Nature*, *392*, 779–787.

Mann, M. E., R. S. Bradley, and M. K. Hughes (1999), Northern hemisphere temperatures during the past millennium: Inferences, uncertainties, and limitations, *Geophys. Res. Lett.*, *26*(6), 759–762.

Matsuno, T., J.-S. Lee, M. Shimizu, S.-H. Kim, and I.-C. Pang (2006), Measurements of the turbulent energy dissipation rate ε and an evaluation of the dispersion process of the Changjiang Diluted Water in the East China Sea, *J. Geophys. Res.*, *111*, C11S09, doi:10.1029/2005JC003196.

McIntyre, S., and R. McKitrick (2003), Corrections to the Mann et al. (1998) "Proxy data base and Northern Hemispheric average temperature models," *Energy Environ.*, *14*, 751–771.

McIntyre, S., and R. McKitrick (2005), Hockey sticks, principal components, and spurious significance, *Geophys. Res. Lett.*, *32*, L03710, doi:10.1029/2004GL021750.

McLeish, W. (1970), Spatial spectra of ocean surface temperature, *J. Geophys. Res.*, *75*, 6872–6877.

Mitchell, J. M. (1976), An overview of climatic variability and its causal mechanisms, *Quat. Res.*, *6*, 481–493.

Moberg, A., D. M. Sonnechkin, K. Holmgren, and N. M. Datsenko (2005), Highly variable Northern Hemisphere temperatures reconstructed from low- and high-resolution proxy data, *Nature*, *433*, 613–617.

Monetti, R. A., S. Havlin, and A. Bunde (2003), Long-term persistence in the sea surface temperature fluctuations, *Physica A*, *320*, 581–589.

Monin, A. S. (1972), *Weather Forecasting as a Problem in Physics*, 216 pp., MIT Press, Boston, Mass.

Monin, A. S., and A. M. Yaglom (1975), *Statistical Fluid Mechanics*, 886 pp., MIT Press, Boston Mass.

Moum, J. N., M. C. Gregg, and R. C. Lien (1995), Comparison of turbulent Kinetic energy dissipation rate estimates from two ocean microstructure profiler, *J. Atmos. Oceanic Technol.*, *12*, 346–366.

Nakajima, H., and N. Hayakawa (1982), A cross-correlation analysis of tidal current, water temperature and salinity records, *J. Oceanogr. Soc. Jpn.*, *38*, 52–56.

Obukhov, A. (1949), Structure of the temperature field in a turbulent flow, *Izv. Akad. Nauk SSSR, Ser. Geogr. Geofiz*, *13*, 55–69.

Obukhov, A. (1959), Effect of archimedean forces on the structure of the temperature field in a turbulent flow, *Dokl. Akad. Nauk SSSR*, *125*, 1246–1248.

Palmén, E. (1959), *The Atmosphere and the Sea in Motion*, edited by B. Bolen, pp. 212–224, Oxford Univ. Press, New York.

Panofsky, H. A. (1969), The spectrum of temperature, *J. Radio Sci.*, *4*(12), 1143–1146.

Parisi, G., and U. Frisch (1985), A multifractal model of intermittency, in *Turbulence and Predictability in Geophysical Fluid Dynamics and Climate Dynamics*, edited by M. Ghil, R. Benzi and G. Parisi, pp. 84–88, North-Holland, Amsterdam, Netherlands.

Pelletier, J. D. (1998), The power spectral density of atmospheric temperature from time scales of 10^{-2} to 10^6 yr, *Earth Planet. Sci. Lett.*, *158*, 157–164.

Peng, C.-K., S. V. Buldyrev, S. Havlin, M. Simons, H. E. Stanley, and A. L. Goldberger (1994), Mosaic organisation of DNA nucleotides, *Phys. Rev. E*, *49*, 1685–1689.

Penland, C. (1996), A stochastic model of IndoPacific sea surface temperature anomalies, *Physica D*, *98*, 534–558.

Peterson, T. C., and R. S. Vose (1997), An overview of the Global Historical Climatology Network temperature database, *Bull. Am. Meteorol. Soc.*, *78*, 2837–2849.

Petit, J. R., et al. (1999), Climate and atmospheric history of the past 420,000 years from the Vostok ice core, Antarctica, *Nature*, *399*, 429–436.

Pinus, N. Z. (1968), The energy of atmospheric macro-turbulence, *Izv. Acad. Sci. USSR Atmos. Oceanic Phys., Engl. Transl.*, *4*, 461.

Radkevitch, A., S. Lovejoy, K. B. Strawbridge, D. Schertzer, and M. Lilley (2008), Scaling turbulent atmospheric stratification. III: Space-time stratification of passive scalars from lidar data, *Q. J. R. Meteorol. Soc.*, *134*, 317–335, doi:10.1002/qj.1203.

Rayner, N. A., et al. (2006), Improved analyses of changes and uncertainties in marine temperature measured in situ since the mid-nineteenth century: The HadSST2 dataset, *J. Clim.*, *19*, 446–469.

Robert, C. W. (1976), Turbulent energy dissipation in the Atlantic equatorial undercurrent, Ph.D. thesis, Univ. of Br. Columbia, Vancouver, B. C., Canada.

Robinson, G. D. (1971), The predictability of a dissipative flow, *Q. J. R. Meteorol. Soc.*, *97*, 300–312.

Rybski, D., A. Bunde, S. Havlin, and H. von Storch (2006), Long-term persistence in climate and the detection problem, *Geophys. Res. Lett.*, *33*, L06718, doi:10.1029/2005GL025591.

Rybski, D., A. Bunde, and H. von Storch (2008), Long-term memory in 1000-year simulated temperature records, *J. Geophys. Res.*, *113*, D02106, doi:10.1029/2007JD008568.

Saunders, P. M. (1972), Space and time variability of temperature in the upper Ocean, *Deep Sea Res. Oceanogr. Abstr.*, *19*, 467–480.

Schertzer, D., and S. Lovejoy (1985a), Generalised scale invariance in turbulent phenomena, *Phys. Chem. Hydrodyn. J.*, *6*, 623–635.

Schertzer, D., and S. Lovejoy (1985b), The dimension and intermittency of atmospheric dynamics, in *Turbulent Shear Flow 4*, edited by B. Launder, pp. 7–33, Springer, Berlin.

Schertzer, D., and S. Lovejoy (1987), Physical modeling and analysis of rain and clouds by anisotropic scaling multiplicative processes, *J. Geophys. Res.*, *92*(D8), 9693–9714.

Schertzer, D., S. Lovejoy, F. Schmitt, Y. Chigirinskaya, and D. Marsan (1997), Multifractal cascade dynamics and turbulent intermittency, *Fractals*, *5*, 427–471.

Schertzer, D., I. Tchiguirinskaia, S. Lovejoy, and A. F. Tuck (2012), Quasi-geostrophic turbulence and generalized scale invariance, a theoretical reply, *Atmos. Chem. Phys.*, *12*, 327–336.

Schmitt, F., S. Lovejoy, and D. Schertzer (1995), Multifractal analysis of the Greenland Ice-Core Project climate data, *Geophys. Res. Lett.*, *22*(13), 1689–1692.

Seuront, L., F. Schmitt, D. Schertzer, Y. Lagadeuc, and S. Lovejoy (1996), Multifractal analysis of Eulerian and Lagrangian variability of physical and biological fields in the ocean, *Nonlin. Processes Geophys.*, *3*, 236–246.

Smith, T. M., R. W. Reynolds, T. C. Peterson, and J. Lawrimore (2008), Improvements to NOAA's historical merged land-ocean surface temperature analysis (1880–2006), *J. Clim.*, *21*, 2283–2293.

Talkner, P., and R. O. Weber (2000), Power spectrum and detrended fluctuation analysis: Application to daily temperatures, *Phys. Rev. E*, *62*, 150–160.

Torrence, T., and G. P. Compo (1998), A practical guide to wavelet analysis, *Bull. Am. Meteorol. Soc.*, *79*, 61–78.

Vallis, G. (2010), Mechanisms of climate variability from years to decades, in *Stochastic Physics and Climate Modelling*, edited by T. Palmer and P. Williams, pp. 1–34, Cambridge Univ. Press, Cambridge, U. K.

Van der Hoven, I. (1957), Power spectrum of horizontal wind speed in the frequency range from .0007 to 900 cycles per hour, *J. Meteorol.*, *14*, 160–164.

Vinnichenko, N. K. (1969), The kinetic energy spectrum in the free atmosphere for 1 second to 5 years, *Tellus*, *22*, 158–166.

Vinnichenko, N., and J. Dutton (1969), Empirical studies of atmospheric structure and spectra in the free atmosphere, *Radio Sci.*, *4*(12), 1115–1126.

Vinther, B. M., H. B. Clausen, D. A. Fisher, R. M. Koerner, S. J. Johnsen, K. K. Andersen, D. Dahl-Jensen, S. O. Rasmussen, J. P. Steffensen, and A. M. Svensson (2008), Synchronizing ice cores from the Renland and Agassiz ice caps to the Greenland Ice Core Chronology, *J. Geophys. Res.*, *113*, D08115, doi:10.1029/2007JD009143.

von Storch, H., E. Zorita, J. M. Jones, Y. Dimitriev, F. González-Rouco, and S. F. B. Tett (2004), Reconstructing past climate from noisy data, *Science*, *306*, 679–682.

Vyushin, D., I. Zhidkov, S. Havlin, A. Bunde, and S. Brenner (2004), Volcanic forcing improves Atmosphere-Ocean Coupled General Circulation Model scaling performance, *Geophys. Res. Lett.*, *31*, L10206, doi:10.1029/2004GL019499.

Witt, A., and A. Y. Schumann (2005), Holocene climate variability on millennial scales recorded in Greenland ice cores, *Nonlin. Processes Geophys.*, *12*, 345–352.

Wunsch, C. (2003), The spectral energy description of climate change including the 100 ky energy, *Clim. Dyn.*, *20*, 353–363.

S. Lovejoy, Department of Physics, McGill University, 3600 University St., Montreal, QC H3A 2T8, Canada. (lovejoy@physics.mcgill.ca)

D. Schertzer, LEESU, Ecole des Ponts ParisTech, Université Paris Est, F-77455 Paris, France.